$C_{43}H_{44}N_2OSi$: C, 81.60; H, 7.01; N, 4.43%. ^{1}H- and ^{13}C-NMR spectra were consistent with those of **11**.

(2*S*,3*R*)-4-Formyl-2,3-methano-1-(1-triphenylmethyl-1*H*-imidazol-4-yl)butane (9)

A mixture of **8** (633 mg, 1.00 mmol) and TBAF (1.0 M THF, 2.0 mL, 2.0 mmol) in THF (6 mL) was stirred at room temperature for 12 h. After the solvent was evaporated, the residue was purified by silica gel column chromatography (50% AcOEt in hexane then 3% MeOH in $CHCl_3$) to give an alcohol product. To a solution of the alcohol in CH_2Cl_2 (10 mL) was added Dess–Martin periodinane (509 mg, 1.20 mmol), and the resulting mixture was stirred at room temperature for 2 h. After addition of saturated aqueous $Na_2S_2O_3$/$NaHCO_3$ (1 : 3), the resulting mixture was stirred vigorously for 10 min. The mixture was extracted with AcOEt, and the organic layer was washed with saturated aqueous $NaHCO_3$, brine, dried (Na_2SO_4), and evaporated. The residue was purified by silica gel column chromatography (33% AcOEt in hexane) to give **9** (305 mg, 78%) as a light brown amorphous solid: $[\alpha]_D^{24}$ −26.0 (*c* 1.00, $CHCl_3$); ^{1}H-NMR (400 MHz, $CDCl_3$) δ 1.04 (1 H, m, cyclopropyl-CH_2), 1.32 (1 H, m, cyclopropyl-CH_2), 1.68–1.83 (2 H, m, cyclopropyl-CH ×2), 2.66 (2 H, d, J = 6.3 Hz, CH_2-imidazole), 6.57 (1 H, s, imidazolyl) 7.12–7.15 (6 H, m, aromatic), 7.32–7.36 (10 H, m, aromatic & imidazolyl), 9.01 (1 H, d, J = 5.3 Hz, C*H*O); ^{13}C-NMR (100 MHz, $CDCl_3$) δ 12.8, 24.2, 27.2, 27.7, 75.1, 117.9, 127.9, 129.6, 138.4, 140.3, 142.5, 201.9; LRMS (EI) *m*/*z* 392 (M^+); HRMS (EI) calcd for $C_{27}H_{24}N_2O$ 392.1889; found 392.1880 (M^+); Found: C, 82.77; H, 6.39; N, 7.18. Calc. for $C_{27}H_{24}N_2O$: C, 82.62; H, 6.16; N, 7.14%.

(2*R*,3*S*)-4-Formyl-2,3-methano-1-(1-triphenylmethyl-1*H*-imidazol-4-yl)butane (*ent*-9)

Compound ***ent*-9** (305 mg, 78%, white amorphous solid) was prepared from ***ent*-8** (633 mg, 1.00 mmol) as described for the preparation of **9**: $[\alpha]_D^{24}$ +25.2 (*c* 1.00, $CHCl_3$); LRMS (EI) *m*/*z* 392 (M^+); HRMS (EI) calcd for $C_{27}H_{24}N_2O$ 392.1889; found 392.1890 (M^+); Found: C, 82.83; H, 6.23; N, 7.42. Calc. for $C_{27}H_{24}N_2O$: C, 82.62; H, 6.16; N, 7.14%. ^{1}H- and ^{13}C-NMR spectra were consistent with those of **9**.

(2*R*,3*R*)-4-Formyl-2,3-methano-1-(1-triphenylmethyl-1*H*-imidazol-4-yl)butane (12)

Compound **12** (259 mg, 65%, white amorphous solid) was prepared from **11** (637 mg, 1.01 mmol) as described for the preparation of **9**: $[\alpha]_D^{23}$ −24.5 (*c* 1.00, $CHCl_3$); ^{1}H-NMR (400 MHz, $CDCl_3$) δ 1.25–1.34 (2 H, m, cyclopropyl-CH_2), 1.83–1.97 (2 H, m, cyclopropyl-CH ×2), 2.67 (1 H, dd, J = 8.2, 15.5 Hz, CH_2-imidazole), 2.95 (1 H, dd, J = 6.3, 15.5 Hz, CH_2-imidazole), 6.53 (1 H, s, imidazolyl) 7.10–7.15 (6 H, m, aromatic), 7.31–7.34 (9 H, m, aromatic), 7.36 (1 H, s, imidazolyl), 9.38 (1 H, d, J = 5.0 Hz, C*H*O); ^{13}C-NMR (100 MHz, $CDCl_3$) δ 15.0, 24.2, 27.2, 27.7, 75.1, 117.9, 127.8, 129.6, 138.4, 140.3, 142.2, 200.9; LRMS (EI) *m*/*z* 392 (M^+); HRMS (EI) calcd for $C_{27}H_{24}N_2O$ 392.1889; found 392.1890 (M^+); Found: C, 82.91; H, 6.00; N, 6.95. Calc. for $C_{27}H_{24}N_2O$: C, 82.62; H, 6.16; N, 7.14%.

(2*S*,3*S*)-4-Formyl-2,3-methano-1-(1-triphenylmethyl-1*H*-imidazol-4-yl)butane (*ent*-12)

Compound ***ent*-12** (290 mg, 65%, a white solid) was prepared from ***ent*-11** (720 mg, 1.14 mmol) as described for the preparation of **9**: $[\alpha]_D^{22}$ +25.0 (*c* 1.05, $CHCl_3$); LRMS (EI) *m*/*z* 392 (M^+); HRMS (EI) calcd for $C_{27}H_{24}N_2O$ 392.1889; found 392.1888 (M^+); Found: C, 82.78; H, 5.97; N, 6.90. Calc. for $C_{27}H_{24}N_2O$: C, 82.62; H, 6.16; N, 7.14%. ^{1}H- and ^{13}C-NMR spectra were consistent with those of **12**.

(2*S*,3*R*)-*trans*-4-(4-Chlorobenzylamino)-2,3-methano-1-(1*H*-imidazol-4-yl)butane (5b)

A mixture of **9** (48 mg, 0.12 mmol), 4-chlorobenzylamine (98%, 16 μL, 0.13 mmol) and 2-picoline borane (13 mg, 0.13 mmol) in MeOH/AcOH (10 : 1, 1.1 mL) was stirred at room temperature for 8 h. After the addition of aqueous HCl (1 M, 1 mL), the mixture was stirred at 0 °C for 10 min and then the solvent was evaporated. The residue was partitioned between Et_2O and aqueous NaOH (2 M), and the organic layer was washed with H_2O, brine, dried (Na_2SO_4), and evaporated. The residue was purified by neutral silica gel column chromatography (10–20% MeOH in $CHCl_3$) to give the crude amine product. A solution of the amine, trityl chloride (56 mg, 0.20 mmol) and Et_3N (28 μL, 0.20 mmol) in CH_2Cl_2 (1 mL) was stirred at room temperature for 12 h. After addition of MeOH (1 mL), the solvent was evaporated. The residue was partitioned between Et_2O and aqueous HCl (0.5 M), and the organic layer was washed with saturated aqueous $NaHCO_3$ and brine, dried (Na_2SO_4), and evaporated. The residue was purified by neutral silica gel column chromatography (17–33% AcOEt in hexane) to give the amine as an amorphous solid. A solution of the amine in EtOH (2.0 mL)/aqueous HCl (4 M, 1.0 mL) was stirred at 78 °C for 2 h, and then the solvent was evaporated. The residue was partitioned between aqueous HCl (1 M) and CH_2Cl_2, and the aqueous layer was neutralized with aqueous NaOH (2 M). The resulting solution was extracted with Et_2O (×3), and the organic layer was washed with H_2O and brine, dried (Na_2SO_4), and evaporated. The residue was purified by Iatron beads column chromatography (0–100% MeOH in $CHCl_3$) to give **5b** (10 mg, 30%, colorless amorphous solid) as a free amine: ^{1}H-NMR (500 MHz, $CDCl_3$) δ 0.47–0.54 (2 H, m, cyclopropyl-CH_2), 0.79–0.86 (2 H, m, cyclopropyl-CH ×2), 2.10–2.17 (2 H, m, CH_2-imidazole), 3.02–3.09 (2 H, m, CH_2NH), 3.75 (1 H, d, J = 13.2 Hz, benzyl-CH_2), 3.84 (1 H, d, J = 13.2 Hz, benzyl-CH_2), 6.77 (1 H, s, imidazolyl), 7.25–7.26 (2 H, m, aromatic), 7.30–7.32 (2 H, m, aromatic) 7.36 (1 H, s, imidazolyl); ^{13}C-NMR (125 MHz, $CDCl_3$) δ 10.2, 17.2, 19.2, 29.3, 53.0, 53.4, 120.9, 128.7, 128.7, 129.6, 129.6, 133.1, 133.1, 134.1, 137.5; LRMS (EI) *m*/*z* 275 (M^+); HRMS (EI) calcd for $C_{15}H_{18}ClN_3$ 275.1189, found 275.1190 (M^+); Found: C, 65.03; H, 6.63; N, 15.49. Calc. for $C_{15}H_{18}ClN_3$: C, 65.33; H, 6.58; N, 15.24%; The free amine **5b** was dissolved in aqueous HCl (4 M), and the solvent was evaporated. The residue was triturated with Et_2O to give **5b dihydrochloride** (12 mg) as a white amorphous solid: $[\alpha]_D^{22}$ −25.2 (*c* 1.01, MeOH); ^{1}H-NMR (400 MHz, CD_3OD) δ 0.76 (2 H, m, cyclopropyl-CH_2), 1.18 (1 H, m, cyclopropyl-CH), 1.24 (1 H, m, cyclopropyl-CH), 2.58 (1 H, dd, J = 7.7, 14.5 Hz, CH_2-imidazole), 2.91–2.96 (2 H, m, CH_2NH), 3.14 (1 H, dd, J = 6.8, 14.5 Hz, CH_2-imidazole), 4.22 (2 H, s, benzyl-CH_2), 7.42 (1 H,

s, imidazolyl), 7.47 (2 H, d, J = 8.2 Hz, aromatic), 7.55 (2 H, d, J = 8.2 Hz, aromatic), 8.83 (1 H, s, imidazolyl); LRMS (EI) m/z 275 [(M–2HCl)$^+$]; HRMS (EI) calcd for $C_{15}H_{18}ClN_3$ 275.1189, found 275.1189 [(M–2HCl)$^+$]; Found: C, 51.52; H, 5.86; N, 11.78. Calc. for $C_{15}H_{20}Cl_3N_3$: C, 51.67; H, 5.78; N, 12.05%.

(2*R*,3*S*)-*trans*-4-(4-Chlorobenzylamino)-2,3-methano-1-(1*H*-imidazol-4-yl)butane (*ent*-5b)

Compound ***ent*-5b** (18 mg, 60%, colorless amorphous solid) was prepared from ***ent*-9** (45 mg, 0.12 mmol) as described for the preparation of **5b**: LRMS (EI) m/z 275 (M$^+$); HRMS (EI) calcd for $C_{15}H_{18}ClN_3$ 275.1189, found 275.1185 (M$^+$); Found: C, 65.00; H, 6.79; N, 15.52. Calc. for $C_{15}H_{18}ClN_3$: C, 65.33; H, 6.58; N, 15.24%; ^{1}H- and ^{13}C-NMR spectra were consistent with those of **5b**; The free amine ***ent*-5b** was dissolved in aqueous HCl (4 M), and the solvent was then evaporated. The residue was triturated with Et_2O to give ***ent*-5b dihydrochloride** (20 mg) as a white amorphous solid: $[\alpha]_D^{22}$ +24.6 (c 1.10, MeOH); LRMS (EI) m/z 275 [(M–2HCl)$^+$]; HRMS (EI) calcd for $C_{15}H_{18}ClN_3$ 275.1189, found 275.1191 [(M–2HCl)$^+$]; Found: C, 51.39; H, 5.98; N, 11.81. Calc. for $C_{15}H_{20}Cl_3N_3$: C, 51.67; H, 5.78; N, 12.05%. ^{1}H-NMR spectrum was consistent with that of **5b dihydrochloride**.

(2*R*,3*R*)-*cis*-4-(4-Chlorobenzylamino)-2,3-methano-1-(1*H*-imidazol-4-yl)butane (6b)

Compound **6b** (27 mg, 49%, colorless amorphous solid) was prepared from **12** (78 mg, 0.20 mmol) as described for the preparation of **5b**: ^{1}H-NMR (500 MHz, $CDCl_3$) δ 0.81 (1 H, dd, J = 5.7, 10.9 Hz, cyclopropyl-CH_2), 0.87 (1 H, m, cyclopropyl-CH_2), 1.02-1.10 (2 H, m, cyclopropyl-CH ×2), 2.08 (1 H, dd, J = 4.6, 15.5 Hz, CH_2-imidazole), 2.40 (1 H, t, J = 12.6 Hz, CH_2NH), 3.15 (1 H, dd, J = 2.3, 15.5 Hz, CH_2-imidazole), 3.34 (1 H, dd, J = 2.9, 12.6 Hz, CH_2NH), 3.78 (1 H, d, J = 12.6 Hz, benzyl-CH_2), 3.93 (1 H, d, J = 12.6 Hz, benzyl-CH_2), 6.76 (1 H, s, imidazolyl), 7.26 (1 H, s, imidazolyl), 7.30 (2 H, d, J = 8.6 Hz, aromatic), 7.35 (2 H, d, J = 8.6 Hz, aromatic); ^{13}C-NMR (125 MHz, $CDCl_3$) δ 8.47, 15.3, 17.1, 24.4, 48.1, 53.0, 123.3, 128.9, 128.9, 129.7, 129.7, 131.3, 133.5, 134.8, 136.9; LRMS (EI) m/z 275 (M$^+$); HRMS (EI) calcd for $C_{15}H_{18}ClN_3$ 275.1189, found 275.1187 (M$^+$); Found: C, 65.10; H, 6.88; N, 14.93. Calc. for $C_{15}H_{18}ClN_3$: C, 65.33; H, 6.58; N, 15.24%; The free amine **6b** was dissolved in aqueous HCl (4 M), and the solvent was then evaporated. The residue was triturated with Et_2O to give **6b dihydrochloride** (30 mg) as a white solid: $[\alpha]_D^{22}$ –11.1 (c 0.96, MeOH); ^{1}H-NMR (400 MHz, CD_3OD) δ 0.56 (1 H, ddd, J = 5.4, 5.9, 11.3 Hz, cyclopropyl-CH_2), 1.06 (1 H, ddd, J = 8.6, 11.3, 12.6 Hz, cyclopropyl-CH_2), 1.36 (1 H, m, cyclopropyl-CH), 1.43 (1 H, m, cyclopropyl-CH), 2.74 (1 H, dd, J = 8.6, 16.3 Hz, CH_2-imidazole), 2.97 (1 H, dd, J = 6.3, 16.3 Hz, CH_2-imidazole), 3.05 (1 H, dd, J = 3.6, 12.7 Hz, CH_2NH), 3.41 (1 H, dd, J = 5.4, 12.7 Hz, CH_2NH), 4.24 (1 H, d, J = 13.1 Hz, benzyl-CH_2), 4.30 (1 H, d, J = 13.1 Hz, benzyl-CH_2), 7.44 (1 H, d, J = 1.1 Hz, imidazolyl), 7.48 (2 H, d, J = 8.6 Hz, aromatic), 7.58 (2 H, d, J = 8.6 Hz, aromatic), 8.84 (1 H, d, J = 1.1 Hz, imidazolyl); LRMS (EI) m/z 275 [(M–2HCl)$^+$]; HRMS (EI) calcd for $C_{15}H_{18}ClN_3$ 275.1189, found 275.1192 [(M–2HCl)$^+$]; Found: C, 51.42; H, 5.95; N, 11.88. Calc. for $C_{15}H_{20}Cl_3N_3$: C, 51.67; H, 5.78; N, 12.05%.

(2*S*,3*S*)-*cis*-4-(4-Chlorobenzylamino)-2,3-methano-1-(1*H*-imidazol-4-yl)butane (*ent*-6b)

Compound ***ent*-6b** (20 mg, 43%, white amorphous solid) was prepared from ***ent*-12** (69 mg, 0.17 mmol) as described for the preparation of **5b**; LRMS (EI) m/z 275 (M$^+$); HRMS (EI) calcd for $C_{15}H_{18}ClN_3$ 275.1189, found 275.1167 (M$^+$); Found: C, 65.14; H, 6.76; N, 15.00. Calc. for $C_{15}H_{18}ClN_3$: C, 65.33; H, 6.58; N, 15.24%; ^{1}H- and ^{13}C-NMR spectra were consistent with those of **6b**; The free amine ***ent*-6b** was dissolved in aqueous HCl (4 M), and the solvent was then evaporated. The residue was triturated with Et_2O to give ***ent*-6b dihydrochloride** (22 mg) as a white solid: $[\alpha]_D^{22}$ +10.8 (c 0.90, MeOH); LRMS (EI) m/z 275 [(M–2HCl)$^+$]; HRMS (EI) calcd for $C_{15}H_{18}ClN_3$ 275.1189, found 275.1188 [(M–2HCl)$^+$]; Found: C, 51.55; H, 5.96; N, 12.13. Calc. for $C_{15}H_{20}Cl_3N_3$: C, 51.67; H, 5.78; N, 12.05%. ^{1}H-NMR spectrum was consistent with that of **6b dihydrochloride**.

(2*S*,3*R*)-*trans*-4-Amino-2,3-methano-1-(1*H*-imidazol-4-yl)butane (5a)

A mixture of **9** (136 mg, 0.347 mmol), (±)-*tert*-butanesulfinamide (59 mg, 0.49 mmol) and anhydrous $CuSO_4$ (560 mg, 3.47 mmol) in CH_2Cl_2 (3 mL) was stirred at room temperature for 24 h. After filtration of the reaction mixture with Celite, the filtrate was evaporated, and the residue was partitioned between $CHCl_3$ and cold aqueous HCl (0.5 M). The organic layer was washed with H_2O and brine, dried (Na_2SO_4), and evaporated. A solution of the residue and added $NaBH_4$ (17 mg, 0.46 mmol) in MeOH (3 mL) was stirred at 0 °C for 2 h. After the solvent was evaporated, the residue was purified by silica gel column chromatography (0–2% MeOH in $CHCl_3$) to give **13** (120 mg, diastereomixture) as a colorless amorphous solid. A mixture of **13** (99 mg) and an EtOH solution of HCl (1 M, 3.0 mL) was stirred at 78 °C for 3 h. After the mixture was evaporated, the residue was washed with Et_2O. The residue was purified by NH silica gel column chromatography (0–20% MeOH in $CHCl_3$) to give **5a** (21 mg, 50% for three steps, colorless amorphous solid) as a free amine: ^{1}H-NMR (500 MHz, CD_3OD) δ 0.41 (2 H, m, cyclopropyl-CH_2), 0.80 (1 H, m, cyclopropyl-CH), 0.87 (1 H, m, cyclopropyl-CH), 2.45–2.55 (4 H, m, CH_2-imidazole & CH_2NH$_2$), 6.78 (1 H, s, imidazolyl), 7.52 (1 H, s, imidazolyl); ^{13}C-NMR (125 MHz, CD_3OD) δ 11.0, 18.2, 21.0, 31.2, 46.2, 117.8, 135.6, 137.4; LRMS (EI) m/z 151 (M$^+$); HRMS (EI) calcd for $C_8H_{13}N_3$ 151.1110, found 151.1100 (M$^+$); Found: C, 63.11; H, 8.89; N, 27.59. Calc. for $C_8H_{13}N_3$: C, 63.54; H, 8.67; N, 27.79%; The free amine **5a** was dissolved in aqueous HCl (4 M), and the solvent was then evaporated. The residue was triturated with Et_2O to give **5a dihydrochloride** (20 mg) as a white amorphous solid: $[\alpha]_D^{22}$ –44.1 (c 1.10, MeOH); ^{1}H-NMR (400 MHz, CD_3OD) δ 0.72 (2 H, m, cyclopropyl-CH_2), 1.12 (1 H, m, cyclopropyl-CH), 1.19 (1 H, m, cyclopropyl-CH), 2.58 (1 H, dd, J = 8.2, 15.9 Hz, CH_2-imidazole), 2.78 (1 H, dd, J = 7.7, 13.1 Hz, CH_2NH$_2$), 2.92 (1 H, dd, J = 6.3, 15.9 Hz, CH_2-imidazole), 2.99 (1 H, dd, J = 7.2, 13.1 Hz, CH_2NH$_2$), 7.42 (1 H, s, imidazolyl), 8.84 (1 H, s, imidazolyl); LRMS (EI) m/z 151 [(M–2HCl)$^+$]; HRMS (EI) calcd for $C_8H_{13}N_3$ 151.1110, found 151.1102 [(M–2HCl)$^+$]; Found: C, 41.50; H, 6.93; N, 17.99. Calc. for $C_8H_{15}Cl_2N_3 \cdot 0.5H_2O$: C, 41.21; H, 6.92; N, 18.02%.

(2*R*,3*S*)-*trans*-4-Amino-2,3-methano-1-(1*H*-imidazol-4-yl)butane (*ent*-5a)

Compound ***ent*-5a** (23 mg, 61% for three steps, colorless amorphous solid) was prepared from ***ent*-9** (99 mg, 0.25 mmol) as described for the preparation of **5a**: LRMS (EI) *m/z* 151 (M^+); HRMS (EI) calcd for $C_8H_{13}N_3$ 151.1110, found 151.1121 (M^+); Found: C, 63.20; H, 8.98; N, 27.48. Calc. for $C_8H_{13}N_3$: C, 63.54; H, 8.67; N, 27.79%; ^{1}H- and ^{13}C-NMR spectra were consistent with those of **5a**; The free amine ***ent*-5a** was dissolved in aqueous HCl (4 M), and the solvent was then evaporated. The residue was triturated with Et_2O to give ***ent*-5a dihydrochloride** (25 mg) as a white amorphous solid: $[\alpha]_D^{22}$ +44.9 (*c* 1.12, MeOH); LRMS (EI) *m/z* 151 [(M–2HCl)$^+$]; HRMS (EI) calcd for $C_8H_{13}N_3$ 151.1110, found 151.1099 [(M–2HCl)$^+$]; Found: C, 42.49; H, 6.82; N, 18.35. Calc. for $C_8H_{15}Cl_2N_3 \cdot 0.1H_2O$: C, 42.53; H, 6.78; N, 18.60%. ^{1}H-NMR spectrum was consistent with that of **5a dihydrochloride**.

(2*R*,3*R*)-*cis*-4-Amino-2,3-methano-1-(1*H*-imidazol-4-yl)butane (6a)

Compound **6a** (18 mg, 59% for three steps, colorless amorphous solid) was prepared from **12** (79 mg, 0.20 mmol) as described for the preparation of **5a**: ^{1}H-NMR (500 MHz, CD_3OD) δ 0.18 (1 H, dd, J = 5.2, 10.9 Hz, cyclopropyl-CH_2), 0.84 (1 H, m, cyclopropyl-CH_2), 1.08–1.19 (2 H, m, cyclopropyl-CH ×2), 2.42 (1 H, dd, J = 8.6, 15.4 Hz, CH_2-imidazole), 2.75 (1 H, dd, J = 9.2, 13.5 Hz, CH_2NH$_2$), 2.87 (1 H, dd, J = 5.2, 15.4 Hz, CH_2-imidazole), 3.05 (1 H, dd, J = 5.7, 13.5 Hz, CH_2NH$_2$), 6.87 (1 H, s, imidazolyl), 7.61 (1 H, d, J = 1.1 Hz, imidazolyl); ^{13}C-NMR (125 MHz, CD_3OD) δ 10.1, 17.1, 18.3, 26.6, 41.6, 117.4, 135.8, 138.4; LRMS (EI) *m/z* 151 (M^+); HRMS (EI) calcd for $C_8H_{13}N_3$ 151.1110, found 151.1109 (M^+); Found: C, 63.11; H, 8.89; N, 27.59. Calc. for $C_8H_{13}N_3$: C, 63.54; H, 8.67; N, 27.79%; The free amine **6a** was dissolved in aqueous HCl (4 M), and the solvent was then evaporated. The residue was triturated with Et_2O to give **6a dihydrochloride** (20 mg) as a white amorphous solid: $[\alpha]_D^{22}$ +2.3 (*c* 0.66, MeOH); ^{1}H-NMR (500 MHz, CD_3OD) δ 0.45 (1 H, dd, J = 5.4, 11.3 Hz, cyclopropyl-CH_2), 1.02 (1 H, m, cyclopropyl-CH_2), 1.31 (1 H, m, cyclopropyl-CH), 1.41 (1 H, m, cyclopropyl-CH), 2.71 (1 H, dd, J = 8.6, 16.3 Hz, CH_2-imidazole), 2.88 (1 H, dd, J = 9.0, 13.1 Hz, CH_2NH$_2$), 3.00 (1 H, dd, J = 6.3, 16.3 Hz, CH_2-imidazole), 3.25 (1 H, dd, J = 5.9, 13.1 Hz, CH_2NH$_2$), 7.44 (1 H, d, J = 0.9 Hz, imidazolyl), 8.86 (1 H, d, J = 1.4 Hz, imidazolyl); LRMS (EI) *m/z* 151 [(M–2HCl)$^+$]; HRMS (EI) calcd for $C_8H_{13}N_3$ 151.1110, found 151.1097 [(M–2HCl)$^+$]; Found: C, 42.60; H, 6.88; N, 18.65. Calc. for $C_8H_{15}Cl_2N_3$: C, 42.87; H, 6.75; N, 18.75%.

(2*S*,3*S*)-*cis*-4-Amino-2,3-methano-1-(1*H*-imidazol-4-yl)butane (*ent*-6a)

Compound ***ent*-6a** (20 mg, 39% for three steps, colorless amorphous solid) was prepared from ***ent*-12** (131 mg, 0.334 mmol) as described for the preparation of **5a**: LRMS (EI) *m/z* 151 (M^+); HRMS (EI) calcd for $C_8H_{13}N_3$ 151.1110, found 151.1095 (M^+); Found: C, 63.39; H, 9.02; N, 27.36. Calc. for $C_8H_{13}N_3$: C, 63.54; H, 8.67; N, 27.79%; ^{1}H- and ^{13}C-NMR spectrum was consistent with that of **6a**; The free amine ***ent*-6a** was dissolved in aqueous HCl (4 M), and the solvent was then evaporated. The residue was triturated with Et_2O to give ***ent*-6a dihydrochloride** (22 mg) as a white solid: $[\alpha]_D^{22}$ –2.2 (*c* 0.58, MeOH); LRMS (EI) *m/z* 151 [(M–2HCl)$^+$]; HRMS (EI) calcd for $C_8H_{13}N_3$ 151.1110, found 151.1121 [(M–2HCl)$^+$]; Found: C, 41.31; H, 6.95; N, 17.93. Calc. for $C_8H_{15}Cl_2N_3 \cdot 0.5H_2O$: C, 41.21; H, 6.92; N, 18.02%. ^{1}H-NMR spectrum was consistent with that of **6a dihydrochloride**.

Binding assay with human histamine receptors

The assay was performed according to the method described previously.[6c] The dihydrochloride salts of the final compounds were used in the assay.

Luciferase reporter gene assay

The assay was performed according to the method described previously.[6b] Briefly, 3 × 10^4 cells of 293-EBNA (Invitrogen) were harvested on collagen-coated 48-well plates for 24 h. An expression plasmid for $G_{\alpha q/i}$, chimera G_α protein of $G_{\alpha q}$ and $G_{\alpha i}$, was constructed and cotransfected with an H_3- or H_4-expression plasmid and a pSRE-Luc. The following day, the cells were treated with histamine (10^{-5} or 10^{-6} M) and/or each compound (10^{-5} M) for 5 h, and laid on ice. Intracellular luciferase activity in aliquots from each lysate was measured using a model ML3000 luminometer (Dynatech Laboratories). The dihydrochloride salts of the final compounds were used in the assay.

Docking simulation

Using the homology modeling of the H_3 receptor that was constructed previously,[6d] the docking simulation was performed according to the method described previously.[6d]

Acknowledgements

This investigation was supported by a Grant-in-Aids for Scientific Research (21390028) from the Japan Society for the Promotion of Science. We are grateful to Sanyo Fine Co., Ltd. for the gift of the chiral epichlorohydrins.

References

1 (*a*) J.-M. Arrang, M. Garbarg and J.-C. Schwartz, *Nature*, 1983, **302**, 832–837; (*b*) *The Histamine H_3 Receptor: A Target for New Drugs*, ed. R. Leurs and H. Timmerman, Elsevier, Amsterdam, 1998; (*c*) R. Leurs, R. A. Bakker, H. Timmerman and I. J. P. de Esch, *Nat. Rev. Drug Discovery*, 2005, **4**, 107–120; (*d*) S. Celanire, M. Wijtmans, P. Talaga, R. Leurs and I. J. P. de Esch, *Drug Discovery Today*, 2005, **10**, 1613–1627; (*e*) T. A. Esbenshade, G. B. Fox and M. D. Cowart, *Mol. Interventions*, 2006, **6**, 77–88.

2 (*a*) M. Krause, H. Stark, and W. Schunack, Medicinal chemistry of histamine H_3 receptor agonists, pp. 175–196. In ref. 1b; (*b*) K. Onodera, and T. Watanabe, Histamine H_3 antagonists as potential therapeutics in the CNS, pp. 255–268. In ref. 1b.

3 (*a*) P. Ling, K. Ngo, S. Nguyen, R. L. Thurmond, J. P. Edwards, L. Karlsson and W. P. Fung-Leung, *Pharmacol.*, 2004, **142**, 161–171; (*b*) W. P. Fung-Leung, R. L. Thurmond, P. Ling and L. Karlsson, *Curr. Opin. Investig. Drugs*, 2004, **11**, 1174–1183; (*c*) H. D. Lim, R. M. van Rijn, P. Ling, R. L. Thurmond, R. A. Bakker and R. Leurs, *J. Pharmacol. Exp. Ther.*, 2005, **314**, 1310–1321.

4 (*a*) T. Klabunde and G. Hessler, *ChemBioChem*, 2002, **3**, 928–944; (*b*) K. Palczewski, T. Kumasaka, T. Hori, C. A. Behnke, H. Motoshima, B. A. Fox, I. Le Trong, D. C. Teller, T. Okada, R. E. Stenkamp, M. Yamamoto and M. Miyano, *Science*, 2000, **289**, 739–745; (*c*) V. Sarramegna, F. Talmont, P. Demange and A. Milon, *Cell. Mol. Life Sci.*, 2003, **60**, 1529–1546; (*d*) S. Schlyer and R. Horuk, *Drug Discovery Today*, 2006, **11**, 481–493; and references therein.

5 Recently, several X-ray crystallographic analyses of GPCR have been reported: (*a*) V. Cherezov, D. M. Rosenbaum, M. A. Hanson, S. G. Rasmussen, F. S. Thian, T. S. Kobilka, H. J. Choi, P. Kuhn, W. I. Weis, B. K. Kobilka and R. C. Stevens, *Science*, 2007, **318**, 1258–1265; (*b*) D. M. Rosenbaum, V. Cherezov, M. A. Hanson, S. G. Rasmussen, F. S. Thian, T. S. Kobilka, H. J. Choi, X. J. Yao, W. I. Weis, R. C. Stevens and B. K. Kobilka, *Science*, 2007, **318**, 1266–1273; (*c*) S. G. Rasmussen, H. J. Choi, D. M. Rosenbaum, T. S. Kobilka, F. S. Thian, P. C. Edwards, M. Burghammer, V. R. Ratnala, R. Sanishvili, R. F. Fischetti, G. F. Schertler, W. I. Weis and B. K. Kobilka, *Nature*, 2007, **450**, 383–387.

6 (*a*) Y. Kazuta, A. Matsuda and S. Shuto, *J. Org. Chem.*, 2002, **67**, 1669–1677; (*b*) Y. Kazuta, K. Hirano, K. Natsume, S. Yamada, R. Kimura, S. Matsumoto, K. Furuichi, A. Matsuda and S. Shuto, *J. Med. Chem.*, 2003, **46**, 1980–1988; (*c*) M. Watanabe, Y. Kazuta, H. Hayashi, S. Yamada, A. Matsuda and S. Shuto, *J. Med. Chem.*, 2006, **49**, 5787–5796; (*d*) M. Watanabe, T. Hirokawa, T. Kobayashi, A. Yoshida, Y. Ito, S. Yamada, N. Orimoto, Y. Yamasaki, M. Arisawa and S. Shuto, *J. Med. Chem.*, 2010, **53**, 3585–3593.

7 The cyclopropane-based stereochemical diversity-oriented strategy was also effectively used for identifying potent proteasome inhibitors: (*a*) K. Yoshida, K. Yamaguchi, T. Sone, Y. Unno, A. Asai, H. Yokosawa, A. Matsuda, M. Arisawa and S. Shuto, *Org. Lett.*, 2008, **10**, 3571–3574; (*b*) K. Yoshida, K. Yamaguchi, A. Mizuno, Y. Unno, A. Asai, T. Sone, H. Yokosawa, A. Matsuda, M. Arisawa and S. Shuto, *Org. Biomol. Chem.*, 2009, **7**, 1868–1877.

8 For examples of the cyclopropane-based conformational restriction, see the following: (*a*) P. D. Armstrong, G. J. Cannon and J. P. Long, *Nature*, 1968, **220**, 65–66; (*b*) K. Shimamoto and Y. Ofune, *J. Med. Chem.*, 1996, **39**, 407–423; (*c*) S. H. Stammer, *Tetrahedron*, 1990, **46**, 2231–2254; (*d*) S. F. Martin, M. P. Dwyer, B. Hartmann and K. S. Knight, *J. Org. Chem.*, 2000, **65**, 1305–1318; (*e*) T. Sekiyama, S. Hatsuya, Y. Tanaka, M. Uchiyama, N. Ono, S. Iwayama, M. Oikawa, K. Suzuki, M. Okunishi and T. Tsuji, *J. Med. Chem.*, 1998, **41**, 1284–1298.

9 (*a*) H. N. C. Wong, M.-Y. Hon, C.-Y. Tse and Y.-C. Yip, *Chem. Rev.*, 1989, **89**, 165–198; (*b*) V. K. Singh, A. DattaGupta and G. Sekar, *Synthesis*, 1997, 137–149; (*c*) M. P. Doyle and M. N. Protopopova, *Tetrahedron*, 1998, **54**, 7919–7946; (*d*) J. Cossy, N. Blanchard and C. Meyer, *Synthesis*, 1999, 1063–1075; (*e*) *Small Ring Compounds in Organic Synthesis VI. Topic in Current Chemistry 207*, A. de Meijere, Ed.; Springer: Berlin, 1999; (*f*) H. Lebel, J.-F. Marcoux, C. Molinaro and A. B. Charette, *Chem. Rev.*, 2003, **103**, 977–1050; (*g*) P. Garcia, D. Diez, A. B. Anton, N. M. Garrido, I. S. Marcos, P. Basabe and J. G. Urones, *Mini-Rev. Org. Chem.*, 2006, **3**, 291–314; (*h*) P. Muller, Y. ves F. Allenbach, S. Chappellet and A Ghanem, *Synthesis*, 2006, **10**, 1689–1696.

10 D. A. Horne, K. Yakushijin and G. A. Buchi, *Heterocycles*, 1994, **39**, 3957–3960.

11 (*a*) R. Kitbunnadaj, O. P. Zuiderveld, I. J. P. de Esch, R. C. Vollinga, R. Bakker, M. Lutz, A. L. Spek, E. Cavoy, M.-F. Deltent, W. M. P. B. Menge, H. Timmerman and R. Leurs, *J. Med. Chem.*, 2003, **46**, 5445–5457; (*b*) R. Kitbunnadaj, M. Hoffmann, S. A. Fratantoni, G. Bongers, R. A. Bakker, K. Wieland, A. el Jilali, I. J. P. de Esch, W. M. P. B. Menge, H. Timmerman and R. Leurs, *Bioorg. Med. Chem.*, 2005, **13**, 6309–6323.

12 An example of an H_3 receptor antagonist having a primary amino function without a hydrophobic group: R. C. Vollinga, W. M. P. B. Menge, R. Leurs and H. Timmerman, *J. Med. Chem.*, 1995, **38**, 266–271.

ARTICLE

Journal of Cellular Biochemistry 113:808–814 (2012)

Journal of Cellular Biochemistry

Identification and Functional Analysis of Zranb2 as a Novel Smad-Binding Protein That Suppresses BMP Signaling

Satoshi Ohte,[1] Shoichiro Kokabu,[1] Shun-ichiro Iemura,[2] Hiroki Sasanuma,[1] Katsumi Yoneyama,[1] Masashi Shin,[1] Seiya Suzuki,[1] Toru Fukuda,[1] Yukio Nakamura,[3] Eijiro Jimi,[4] Toru Natsume,[2] and Takenobu Katagiri[1]*

[1]*Division of Pathophysiology, Research Center for Genomic Medicine, Saitama Medical University, 1397-1 Yamane, Hidaka-shi, Saitama, 350-1241, Japan*

[2]*Biological Systems Control Team, Biomedicinal Information Research Center, National Institute of Advanced Industrial Science and Technology, 2-42 Aomi, Koto-ku, Tokyo, 135-0064, Japan*

[3]*Showa Inan General Hospital, 3230 Akaho, Komagane-shi, Nagano, 399-4117, Japan*

[4]*Department of Biosciences, Kyushu Dental College, Kitakyushu-shi, Fukuoka, 803-8580, Japan*

ABSTRACT

Smads 1/5/8 transduce the major intracellular signaling of bone morphogenetic proteins (BMPs). In the present study, we analyzed Smad1-binding proteins in HEK293T cells using a proteomic technique and identified the protein, zinc-finger, RAN-binding domain-containing protein 2 (ZRANB2). Zranb2 interacted strongly with Smad1, Smad5, and Smad8 and weakly with Smad4. The overexpression of Zranb2 inhibited BMP activities in C2C12 myoblasts *in vitro*, and the injection of Zranb2 mRNA into zebrafish embryos induced weak dorsalization. Deletion analyses of Zranb2 indicated that the serine/arginine-rich (SR) domain and the glutamine-rich domain were required for the inhibition of BMP activity and the interaction with Smad1, respectively. Zranb2 was found to be localized in the nucleus; however, the SR domain-deleted mutant localized to the cytoplasm. The knockdown of endogenous Zranb2 in C2C12 cells enhanced BMP activity. Zranb2 suppressed Smad transcriptional activity without affecting Smad phosphorylation, nuclear localization, or DNA binding. Taken together, these findings suggested that Zranb2 is a novel BMP suppressor that forms a complex with Smads in the nucleus. J. Cell. Biochem. 113: 808–814, 2012.

KEY WORDS: BMP; SMAD; ZRANB2; PROTEIN INTERACTION; SIGNAL TRANSDUCTION

Bone morphogenetic proteins (BMPs) are multifunctional growth factors that are members of the transforming growth factor-β family. BMPs exhibit a unique activity in bone matrix that is characterized by ectopic bone formation in muscle tissues *in vivo* [Urist, 1965]. BMPs inhibit the myogenic differentiation of myoblasts and cause an osteogenic differentiation into osteoblastic lineage cells *in vitro* [Katagiri et al., 1994]. BMPs physiologically regulate bone formation and the development and regeneration of various tissues in vertebrates and lower animals [Katagiri et al., 2008]. In zebrafish and Xenopus embryos, BMP signaling plays an important role in the determination of a dorsal–ventral axis during development [Suzuki et al., 1994; Nakamura et al., 2007].

BMP signaling is transduced using two different transmembrane serine/threonine kinase receptors, which are termed type I and type II receptors [Miyazono et al., 2005; Wan and Cao, 2005]. The BMP-bound type II receptor phosphorylates the type I receptor. The activated BMP type I receptor kinase subsequently phosphorylates a serine–valine–serine (SVS) motif at the C-termini of Smad1, Smad5, and Smad8, which are the BMP receptor-regulated Smads (R-Smads) [Katagiri, 2010]. The phosphorylated R-Smads form heteromeric complexes with Smad4, which is a common Smad (Co-Smad), and translocate into the nucleus to regulate the transcription of direct target genes, such as *Id1* [Katagiri et al., 2002]. A GC-rich element in the 5′ enhancer region of the *Id1* gene has been identified as the BMP-responsive element (BRE), which is recognized by a complex of BMP-regulated Smads and Smad4 in response to activation of the BMP type I receptor. The overexpression of a constitutively active Smad1, in which the SVS motif has been substituted with a DVD

Grant sponsor: Ministry of Health, Labour and Welfare of Japan; Grant number: H23-nanchi-ippan-032; Grant sponsor: Ministry of Education, Culture, Sports, Science, and Technology of Japan; Grant numbers: 21390423, 23659732, 21890243, S0801004; Grant sponsor: Takeda Science Foundation; Grant number: 2009-Katagiri.

*Correspondence to: Takenobu Katagiri, Division of Pathophysiology, Research Center for Genomic Medicine, Saitama Medical University, 1397-1 Yamane, Hidaka-shi, Saitama, 350-1241, Japan. E-mail: katagiri@saitama-med.ac.jp

Received 8 September 2011; Accepted 6 October 2011 • DOI 10.1002/jcb.23408 • © 2011 Wiley Periodicals, Inc.
Published online 20 October 2011 in Wiley Online Library (wileyonlinelibrary.com).

sequence, activates the expression of the *Id1* reporter gene and the osteoblastic differentiation of myoblasts in the absence of BMPs [Nojima et al., 2010]. Moreover, a chemical inhibitor of BMP type I receptor-mediated R-Smad phosphorylation suppressed BMP receptor-mediated osteoblastic differentiation and heterotopic bone formation [Yu et al., 2008a, b]. These findings suggest that Smads play a critical role in BMP activities both *in vitro* and *in vivo*.

The activity of Smad proteins is regulated via interactions with various factors, including modifying enzymes, co-activators, and co-repressors [Miyazono et al., 2006]. The Smads are degraded by binding to the ubiquitin–proteasome system *via* interactions with E3 ubiquitin ligases, such as Smad ubiquitin regulatory factors 1 and 2 (Smurf1 and Smurf2) [Zhu et al., 1999]. In addition, two distinct phosphatases, small C-terminal domain phosphatases (SCPs) and protein phosphatase magnesium-dependent 1A (PPM1A), have been identified as enzymes that stimulate the dephosphorylation of Smads [Knockaert et al., 2006; Lin et al., 2006]. In the nucleus, Smads interact with various transcriptional co-activators, including p300, CBP, and PCAF [Feng et al., 1998; Itoh et al., 2000], and co-repressors, including Ski, SnoN, and YY1 [Akiyoshi et al., 1999; Wu et al., 2002; Kurisaki et al., 2003]. Thus, the identification and characterization of novel Smad-binding proteins are important to understand the mechanisms of the Smad signaling pathway. In the present study, we report the identification and characterization of a protein, zinc-finger, RAN-binding domain containing protein 2 (Zranb2), as a factor that binds BMP-regulated R-Smads. Zranb2, also known as Zis and Znf265, was identified previously in renal juxtaglomerular cells [Karginova et al., 1997]. Zranb2 contains two RanBP2-type zinc-finger domains, a glutamic acid-rich (Glu) region and a C-terminal Ser/Arg-rich (SR) domain [Mangs and Morris, 2008]. Zranb2 is involved in the alternative splicing of RNA through the zinc-finger domains in a reconstituted assay *in vitro* [Adams et al., 2001]. The current study is the first report to demonstrate that Zranb2 acts as a BMP inhibitor by suppressing Smad transcriptional activity without affecting Smad phosphorylation or DNA-binding capacity.

RESULTS

ZRANB2 INTERACTS WITH BMP-REGULATED SMADS

To identify novel proteins that regulate BMP signaling *via* the Smads, we analyzed Smad1-binding proteins using a proteomic technique. FLAG-Smad1 was overexpressed in HEK293T cells, and the Smad1-binding proteins were enriched from whole-cell extracts using immunoprecipitation with an anti-FLAG antibody. ZRANB2 was identified as a Smad1-binding protein (Fig. 1A). Myc-tagged Zranb2 interacted with FLAG-Smad1 and weakly interacted with FLAG-Smad4 in HEK293T cells (Fig. 1B), and this binding capacity of Zranb2 to Smad1 was not affected by BMP-4 stimulation (Fig. 1C). In addition, Zranb2 interacted with two other BMP-regulated R-Smads, Smad5 and Smad8 (Fig. 1D).

ZRANB2 INHIBITS BMP ACTIVITIES VIA SMADS

We examined the effect of Zranb2 on BMP activities in C2C12 myoblasts, a well-characterized model system for studying the biological activity of BMPs [Katagiri et al., 1994]. The ALP activity

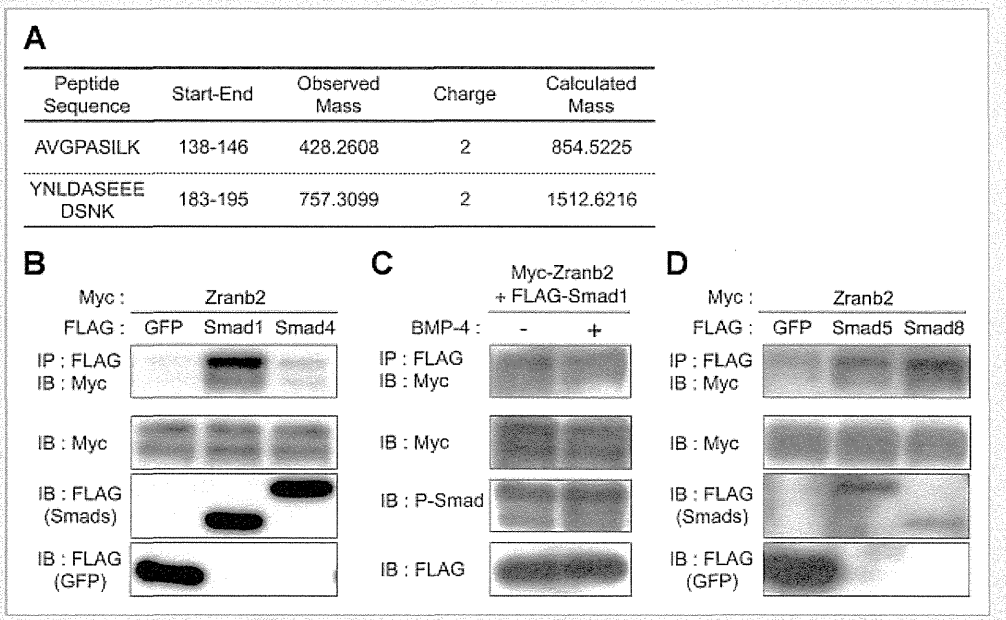

Fig. 1. Zranb2 interacts with Smads. A: Identification of ZRANB2 by LC-MS/MS analysis. The amino acid sequence assigned to each peptide and its position in the ZRANB2 sequence. Also indicates observed mass and charge of the peptide ion together with calculated mass. B, D: HEK293T cells were co-transfected with Myc-tagged Zranb2 and Flag-tagged Smad1 or Smad4 (B), Flag-tagged Smad5 or Smad8 (D) constructs. Whole cell lysates were immunoprecipitated (IP) with an α-FLAG antibody and immunoblotted with an α-Myc antibody. C: HEK293T cells were transfected with Myc-Zranb2 and Flag-Smad1 and treated for 1 h with or without 100 ng/ml BMP-4. Whole cell lysates were IP with an α-FLAG antibody and immunoblotted with an α-Myc antibody.

and *Osterix* mRNA expression were measured as typical markers of the osteoblastic differentiation that is induced by BMP activity. The overexpression of Zranb2 suppressed the ALP activity and osterix mRNA, which were induced by the transient transfection of constitutively active BMPR-IA, BMPR-IA(Q233D), and Smad1 (Fig. 2A,B). The overexpression of Zranb2 also suppressed Id1WT4F luciferase reporter activity that was driven by the BRE in the *Id1* gene following BMP-4 stimulation (Fig. 2C). We observed that Zranb2 exhibited similar suppression profiles on the BMP activity in both osteoblastic MC3T3-E1 cells and primary osteoblasts (data not shown). The injection of synthetic Zranb2 mRNA into *Danio rerio* (zebrafish) embryos caused approximately 4.4% dorsalized embryos, indicating that Zranb2 has a weak BMP-inhibitory effect in developing zebrafish (Fig. 2D,E). This result was surprising since we likely expect approximately more than 50% phenotypic consequences when target genes are mutated in zebrafish [Nakamura et al., 2007]. These results suggest that Zranb2 acts as a suppressor of BMP activity in mammalian cells and in *Danio rerio* embryos.

THE SR DOMAIN OF ZRANB2 IS ESSENTIAL FOR THE INHIBITION OF BMP SIGNALING

The primary sequence of Zranb2 predicts several structurally distinct domains: Two zinc-fingers (ZFs), a glutamic acid (Glu)-rich domain, and a serine and arginine-rich (SR) domain. To identify the domain of Zranb2 that is crucial for BMP inhibition, we generated a series of deletion mutants of Myc-Zranb2 lacking the ZFs and/or the Glu and/or SR domains (Fig. 3A). Our immunohistochemical analysis using an anti-Myc antibody indicated that the ΔZF1, ΔZF, and SR mutants were localized in the nucleus and suppressed the BMP activity similar to the wild-type Zranb2 (Fig. 3B,C). However, the ΔSR mutant was mainly localized in the cytoplasm and showed a slight enhancement, rather than an inhibition, of BMP signaling (Fig. 3B,C). We further examined the interactions of these mutants with Smad1 in a co-immunoprecipitation assay. Unexpectedly, the ΔSR mutant bound to Smad1 despite the loss of the BMP inhibition (Fig. 3D). In contrast, the SR mutant did not interact with Smad1 but suppressed BMP activity (Fig. 3D). These results suggest that the Glu and SR domains may be required for Smad interactions and BMP inhibition, respectively (see the Discussion section). In addition, we demonstrated that the MH2 domain of Smad1 was a Zranb2-interacting domain (Fig. 3E).

ZRANB2 SUPPRESSES THE TRANSCRIPTIONAL ACTIVITY OF SMADS WITHOUT INHIBITING THEIR DNA-BINDING ACTIVITY

To clarify the molecular mechanisms of Zranb2, we examined the effect of Zranb2 on the early events that are induced by BMP signaling, which include Smad phosphorylation and nuclear localization. Equivalent levels of phosphorylated Smad1/5/8 that were induced by BMPR-IA(Q233D) were detected in the presence and absence of Zranb2 (Fig. 4A). We demonstrated that phosphorylated Smad1/5/8 were localized in the nuclei in Zranb2-negative and Zranb2-overexpressing cells (Fig. 4B). Moreover, Zranb2 suppressed the BMP-specific luciferase reporter activity that was induced by the constitutively activated Smad1, Smad1(DVD), which activates the transcription of target genes, regardless of the phosphorylation status (Fig. 4C). These results suggest that the BMP receptor-mediated phosphorylation of Smad1/5/8 is not the targeted event of Zranb2-mediated suppression.

We also investigated the role of endogenous Zranb2 on the BMP activity in C2C12 cells. Transfection of two types of siRNAs against mouse Zranb2 but not scramble siRNA reduced the Zranb2 protein levels and enhanced the Id1WT4F luciferase reporter activity

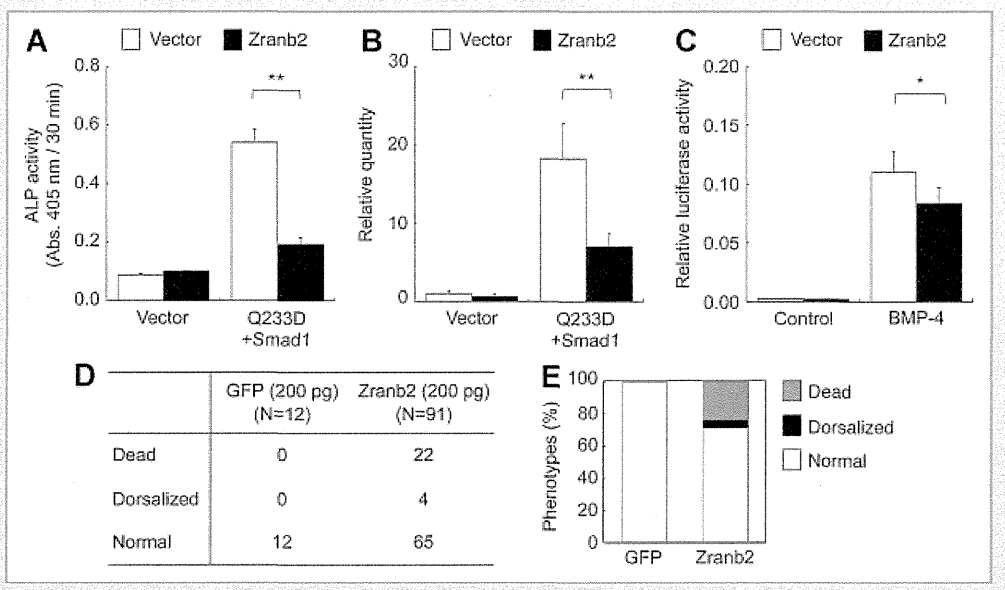

Fig. 2. Zranb2 inhibits BMP activity. A, B: ALP activity (A) or *Osterix* mRNA expression (B) was induced by the overexpression of constitutively active BMPR-IA (Q233D) with Smad1 in the presence or absence of Zranb2 in C2C12 cells. C: Id1WT4F-luc activity was induced by BMP-4 (5 ng/ml) in C2C12 cells that were transfected with or without Zranb2. D, E: Zranb2 induces weak dorsalization of the zebrafish embryo; synthetic Zranb2 mRNA (200 pg) was injected into the embryos. Results are presented as the mean ± SD ($n = 3$), $^{*}P < 0.05$ and $^{**}P < 0.01$ compared with control.

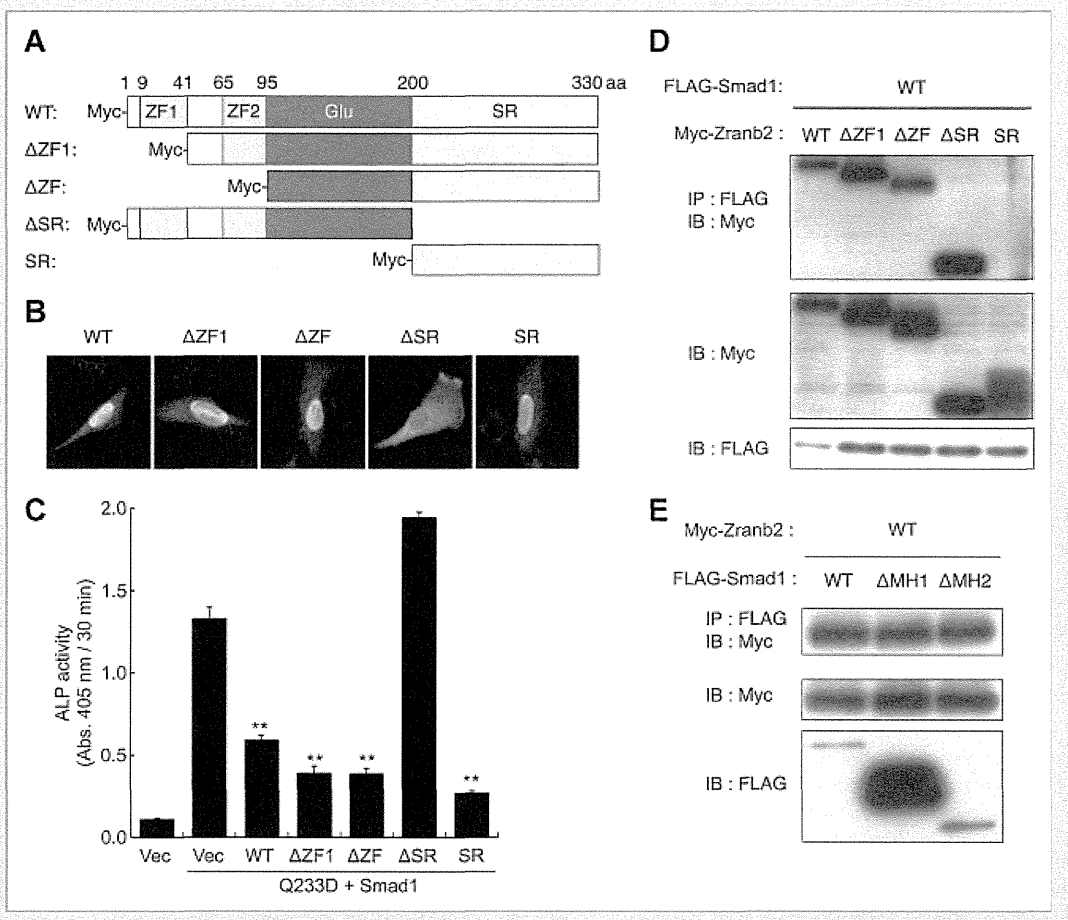

Fig. 3. The SR domain of Zranb2 is important for the inhibition of BMP activity. A: Construction of the deletion mutants of Zranb2. ZF1 and ZF2, zinc finger domains; Glu, a glutamic acid-rich domain; and SR, a serine and arginine-rich domain. B: Cellular localization of the Zranb2 mutants. C2C12 cells were transfected with one of the Zranb2 mutants followed by immunofluorescent staining with an α-Myc antibody. Original magnification, ×40. C: The SR domain suppressed the BMP activity. The ALP activity was induced by the overexpression of BMPR-IA(Q233D) and Smad1 in the presence or absence of Zranb2 in C2C12 cells. D: Analysis of the binding capacities of the Zranb2 mutants to Smad1. HEK293T cells were co-transfected with FLAG-tagged Smad1 and one of the Myc-tagged Zranb2 constructs. Whole-cell lysates were immunoprecipitated with an α-FLAG antibody and immunoblotted with an α-Myc antibody. E: The analysis of the binding capacities of the MH1 and MH2 domains of Smad1 to Zranb2. HEK293T cells were co-transfected with Myc-tagged Zranb2 and Flag-tagged Smad1(ΔMH1) or Smad1(ΔMH2). Whole cell lysates were immunoprecipitated with an α-FLAG antibody and immunoblotted with an α-Myc antibody. Results are presented as the mean ± SD (n = 3), $^{*}P < 0.05$ and $^{**}P < 0.01$ compared with control.

(Fig. 4D,E). These results suggest that Zranb2 physiologically suppresses BMP activity. However, equivalent amounts of phosphorylated Smad1/5/8 were bound to the BRE in a DNA-precipitation assay in the presence and absence of Zranb2 siRNAs. These results suggest that Zranb2 does not block the DNA-binding capacity of Smads (Fig. 4D). In addition, Zranb2 itself was not found to interact with the BRE (Fig. 4D).

DISCUSSION

In the present study, we identified Zranb2 as a novel inhibitor of BMP activity via interactions with BMP-specific Smads. Zranb2 suppressed the BMP activity in mammalian cells *in vitro* and zebrafish embryos *in vivo*. These results suggest that Zranb2 may act as an inhibitor of BMP activity in vertebrates. This is the first report demonstrating interactions between Zranb2 and BMP signaling.

Zranb2 is an SR domain-containing nuclear protein that is ubiquitously expressed in various tissues and is conserved from nematodes to mammals [Karginova et al., 1997; Mangs and Morris, 2008]. The SR proteins are splicing factors that contain a C-terminal SR domain and an N-terminal RNA recognition ZF motif [Shen and Green, 2006]. Zranb2 recognizes RNA *via* its N-terminal ZF motifs and regulates alternative splicing in a reconstituted model *in vitro* [Loughlin et al., 2009]. However, our deletion study showed that the ZF motifs were not essential for BMP inhibition or Smad1 binding. These results suggest that the alternative splicing of RNA may not be involved in Zranb2-mediated inhibition of BMP activity. In contrast, the SR domain of Zranb2 was essential for the nuclear localization and the inhibition of BMP activity. However, this SR domain did not interact with Smad1. The Glu-rich domain may be involved in interactions with the Smad1 MH2 domain. Although ZRANB1 and ZRANB3 share conserved ZF motifs with ZRNAB2, their amino acid sequences do not show a significant similarity with the Glu-rich

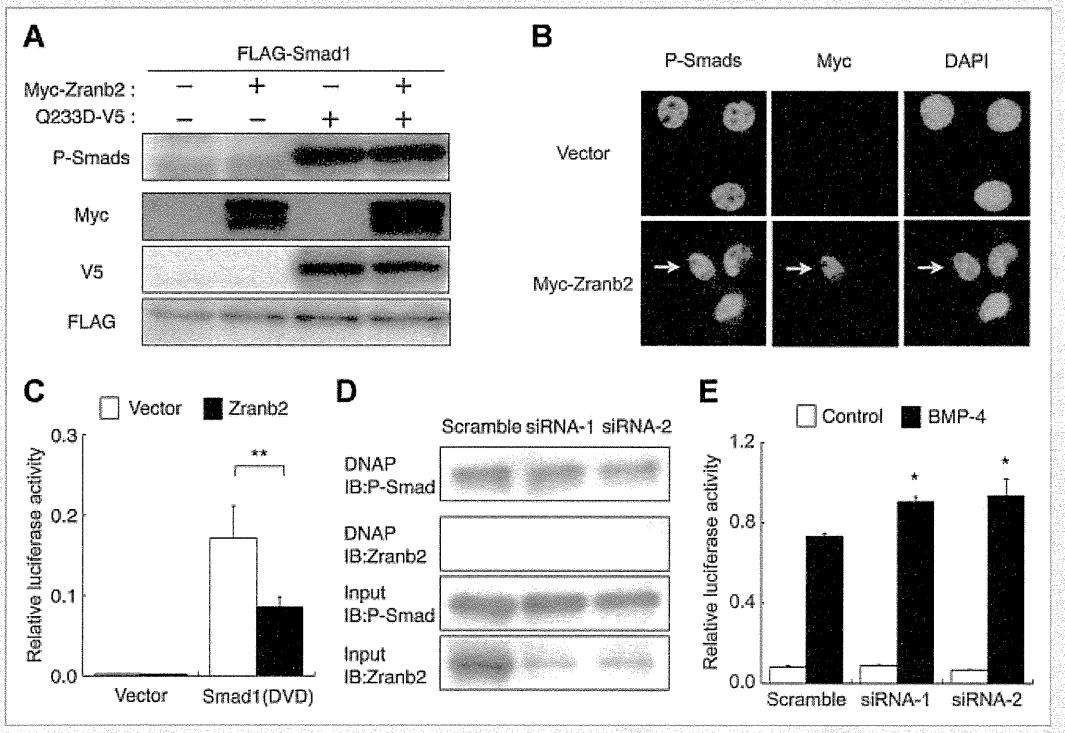

Fig. 4. Zranb2 inhibits the transcriptional activity of Smads without suppressing their DNA-binding capacity. A: Western blot analysis. C2C12 cells were co-transfected with FLAG-tagged Smad1 with or without Myc-tagged Zranb2 and V5-tagged BMPR-IA(Q233D). Whole cell lysates were immunoblotted with α-phospho-Smad1/5/8, α-FLAG, α-Myc, or α-V5 antibodies. B: C2C12 cells were transfected with Myc-tagged Zranb2 or empty vector and treated for 1 h with BMP-4 (100 ng/ml) and stained with α-phospho-Smad1/5/8 or α-Myc antibodies. Original magnification, ×40. C: Zranb2 inhibited the BMP-specific IdWT4F-luc activity that was induced by the constitutively activated Smad1, Smad1DVD. D, E: Effects of Zranb2 siRNA knockdown on the BMP activity and DNA binding of Smads. C2C12 cells were transfected with Zranb2 siRNA or scrambled siRNA. D: Nuclear extracts were affinity precipitated using the BRE and immunoblotted with α-phospho-Smad1/5/8 or α-Zranb2 antibodies. E: BMP-specific luciferase activity was induced by BMP-4. Results are presented as the mean ± SD (n = 3), $^{*}P < 0.05$ and $^{**}P < 0.01$ compared with control.

domain, SR domain, or other regions of ZRANB2 [Evans et al., 2001; Wiemann et al., 2001]. The Glu-rich and SR domains are important for the Zranb2-mediated inhibition of BMP signaling. Therefore, we hypothesized that the inhibition of BMP signaling may be unique to Zranb2 among these ZF motif-containing proteins.

Zranb2 inhibited the BMP-induced osteoblastic differentiation of the C2C12 cells and the BMP-specific luciferase reporter activity that was driven by the BRE in the *Id1* gene. However, Zranb2 did not affect the phosphorylation levels or nuclear localization of the Smads. Moreover, the DNA-binding capacity of Smads in response to BMP stimulation was not changed by the presence or absence of Zranb2, suggesting that another mechanism is involved in Zranb2-mediated inhibition. According to our results, Zranb2 interacts with the Smad1 MH2 domain, which is important for interactions with other co-activators and co-repressors, such as Smad4, p300/CBP, c-Ski, and YY1. A previous study has reported that Zranb2 co-localizes with p300 and YY1 in the nucleus [Adams et al., 2001]. Thus, it may be possible that Zranb2 outcompetes a co-activator that is essential for the transcription of target genes or recruits a co-repressor to the Smad-DNA complex on the BRE. We showed that Zranb2 was not detected on the BRE in a DNAP assay. This result supports the possibility of competition between Zranb2 and co-activators. Further studies are needed to identify and elucidate the detailed molecular mechanisms, including the critical target molecules of Zranb2 that mediate Zranb2-dependent BMP inhibition.

In conclusion, Zranb2 is a novel BMP suppressor that forms a complex with Smads in the nucleus. Our findings provide new insight into the molecular mechanisms of BMP signaling.

MATERIAL AND METHODS

Immunopurification and mass spectrometry. The FLAG-tagged Smad1 plasmid that is described below was transfected into HEK293T cells. The cytosolic extraction and immunoprecipitation procedures were performed as previously described [Komatsu et al., 2004]. The eluates from the immunoprecipitates were analyzed using nanoscale LC-MS/MS system as described previously [Natsume et al., 2002].

Plasmid constructs. Plasmids encoding the wild-type Smads, constitutively active BMPR-IA(Q233D), constitutively active Smad1(DVD), and IdWT4F-luc have been previously described [Nojima et al., 2010], [Fukuda et al., 2008]. The wild-type and mutated mouse Zranb2 (Accession number NM_017381) derivatives were obtained using standard RT-PCR techniques with PrimeStar HS DNA polymerase (TaKaRa, Shiga, Japan) and cloned into a pcDEF3 expression vector [Goldman et al., 1996]. All of the final constructs were confirmed by sequencing.

Cell culture, transfection, ALP assay, and the luciferase reporter assay. HEK293T human kidney cells, C2C12 mouse myoblasts, C3H10T1/2 mouse fibroblasts, and MC3T3-E1 mouse osteoblasts were maintained as previously described [Kokabu et al., 2011; Ohte et al., 2011]. The cells were transfected with the indicated plasmids using Lipofectamine 2000 (Invitrogen, Carlsbad, CA) according to the manufacturer's instructions. The ALP activity was measured as a marker of osteoblast differentiation as previously described [Kodaira et al., 2006]. The luciferase reporter assay was performed using IdWT4F-luc and phRL-SV40 (Promega, Madison, WI) with the Dual-Glo Luciferase Assay system (Promega) as previously described [Katagiri et al., 2002].

Immunohistochemistry, western blot, and immunoprecipitation. The following antibodies were used for the immunohistochemistry, immunoprecipitation, and western blot analysis: α-FLAG (clone M2, Sigma, St Louis, MO), polyclonal α-Myc (Medical & Biological Laboratories, Nagoya, Japan), α-V5 (clone V5005, Nacalai Tesque, Kyoto, Japan), polyclonal α-phosphorylated Smad1/5/8 (Cell Signaling Technology, Beverly, MA), polyclonal α-ZNF265(Zranb2) (E-16, Santa Cruz Biotechnology, Heidelberg, Germany), and α-MHC (clone MF-20, Developmental Studies Hybridoma Bank, Iowa City, IA). For the immunohistochemical analysis, the target proteins were visualized using the Alexa488- or Alexa594-conjugated secondary antibodies (Invitrogen). The western blot analysis was performed as previously described [Fukuda et al., 2009]. The target proteins were immunoprecipitated for 3 h at 4°C using M2-agarose beads (Sigma).

Injection of synthetic RNA into zebrafish embryos. The full-length Zranb2 sequence was cloned into the pCS2+ expression vector, and RNA was synthesized from NotI-digested pCS2+ plasmids using the SP6 mMessage mMachine kit (Ambion, Austin, TX). Phenol red (0.1%) was added to the RNA solution as a tracer, and the RNA (200 pg) was injected into 1–2 cell-stage embryos. Following the injection, the embryos were cultured in aquatic system water and imaged as previously described [Nakamura et al., 2007].

DNA affinity precipitation. The DNA affinity precipitation was performed as previously described, with some modifications [Suzuki et al., 1993]. Nuclear extracts from the C2C12 cells were prepared using the ProteoJET cytoplasmic and nuclear protein extraction kit (Fermentas, Glen Burnie, MD). The biotinylated DNA probes were prepared using PCR with biotin-conjugated primers. The biotinylated DNA probe (1 μg) and nuclear extracts (100 μg of protein) were incubated for 30 min on ice in a volume (500 μl) of a solution containing 20 mM HEPES–KOH (pH 7.9), 80 mM KCl, 1 mM $MgCl_2$, 0.2 mM EDTA, 0.5 mM DTT, 5%(v/v) glycerol, protease inhibitor cocktail (Roche Diagnostics GmbH, Mannheim, Germany), and phosphatase inhibitor (Nacalai Tesque). Dynabeads M-280 streptavidin (Invitrogen) were added and mixed by rotation for 1 h at 4°C. The collected proteins were subjected to western blot analysis as described above.

Reverse transcriptase PCR and real-time PCR analysis. Total RNA was isolated using TRIzol (Invitrogen) and reverse-transcribed into cDNA using Superscript III (Invitrogen). The cDNA was amplified using PCR with specific primers for *Osterix*, *Alp*, *Osteocalcin*, and *Atp5f1* (TaKaRa). *Atp5f1* was used as control. SYBR green-based real-time PCR was performed in a 96-well plate format SYBR Premix Ex Taq (TaKaRa) and a Thermal Cycler Dice Real-time system TP800 (TaKaRa).

Statistical analysis. An unpaired Student's *t*-test was used for the comparisons. The data are expressed as the mean ± SD, and the statistical significance is indicated as $^{*}P < 0.05$ and $^{**}P < 0.01$.

ACKNOWLEDGMENTS

The authors are grateful to Dr. J. A. Langer for kindly providing pcDEF3. This work was supported in part by Health and Labour Sciences Research Grants for Research on Measures for Intractable Research from the Ministry of Health, Labour and Welfare of Japan, grants-in-aid from the Ministry of Education, Culture, Sports, Science, and Technology of Japan, a grant-in-aid from the Takeda Science Foundation, and a grant-in-aid for the "Support Project of Strategic Research Center in Private Universities" from the Ministry of Education, Culture, Sports, Science and Technology (MEXT) to Saitama Medical University Research Center for Genomic Medicine.

REFERENCES

Adams DJ, van der Weyden L, Mayeda A, Stamm S, Morris BJ, Rasko JE. 2001. ZNF265–a novel spliceosomal protein able to induce alternative splicing. J Cell Biol 154:25–32.

Akiyoshi S, Inoue H, Hanai J, Kusanagi K, Nemoto N, Miyazono K, Kawabata M. 1999. c-Ski acts as a transcriptional co-repressor in transforming growth factor-beta signaling through interaction with smads. J Biol Chem 274: 35269–35277.

Evans PC, Taylor ER, Coadwell J, Heyninck K, Beyaert R, Kilshaw PJ. 2001. Isolation and characterization of two novel A20-like proteins. Biochem J 357:617–623.

Feng XH, Zhang Y, Wu RY, Derynck R. 1998. The tumor suppressor Smad4/DPC4 and transcriptional adaptor CBP/p300 are coactivators for smad3 in TGF-beta-induced transcriptional activation. Genes Dev 12:2153–2163.

Fukuda T, Kanomata K, Nojima J, Kokabu S, Akita M, Ikebuchi K, Jimi E, Komori T, Maruki Y, Matsuoka M, Miyazono K, Nakayama K, Nanba A, Tomoda H, Okazaki Y, Ohtake A, Oda H, Owan I, Yoda T, Haga N, Furuya H, Katagiri T. 2008. A unique mutation of ALK2, G356D, found in a patient with fibrodysplasia ossificans progressiva is a moderately activated BMP type I receptor. Biochem Biophys Res Commun 377:905–909.

Fukuda T, Kohda M, Kanomata K, Nojima J, Nakamura A, Kamizono J, Noguchi Y, Iwakiri K, Kondo T, Kurose J, Endo KI, Awakura T, Fukushi J, Nakashima Y, Chiyonobu T, Kawara A, Nishida Y, Wada I, Akita M, Komori T, Nakayama K, Nanba A, Maruki Y, Yoda T, Tomoda H, Yu PB, Shore EM, Kaplan FS, Miyazono K, Matsuoka M, Ikebuchi K, Akira O, Hiromi O, Eijiro J, Ichiro O, Yasushi O, Takenobu K. 2009. Constitutively activated ALK2 and increased smad1/5 cooperatively induce BMP signaling in fibrodysplasia ossificans progressiva. J Biol Chem 284:7149–7156.

Goldman LA, Cutrone EC, Kotenko SV, Krause CD, Langer JA. 1996. Modifications of vectors pEF-BOS, p cDNA1 and pcDNA3 result in improved convenience and expression. Biotechniques 21:1013–1015.

Itoh S, Ericsson J, Nishikawa J, Heldin CH, ten Dijke P. 2000. The transcriptional co-activator P/CAF potentiates TGF-beta/Smad signaling. Nucleic Acids Res 28:4291–4298.

Karginova EA, Pentz ES, Kazakova IG, Norwood VF, Carey RM, Gomez RA. 1997. Zis: A developmentally regulated gene expressed in juxtaglomerular cells. Am J Physiol 273:F731–F738.

Katagiri T, Imada M, Yanai T, Suda T, Takahashi N, Kamijo R. 2002. Identification of a BMP-responsive element in Id1, the gene for inhibition of myogenesis Genes Cells 7:949–960.

Katagiri T, Suda T, Miyazono K. 2008. The bone morphogenetic proteins. New York: Cold Spring Harbor Press.

Katagiri T, Yamaguchi A, Komaki M, Abe E, Takahashi N, Ikeda T, Rosen V, Wozney JM, Fujisawa-Sehara A, Suda T. 1994. Bone morphogenetic protein-2 converts the differentiation pathway of C2C12 myoblasts into the osteoblast lineage. J Cell Biol 127:1755–1766.

Katagiri T. 2010. Heterotopic bone formation induced by bone morphogenetic protein signaling: Fibrodysplasia ossificans progressiva. J Oral Biosci 52:33–41.

Knockaert M, Sapkota G, Alarcon C, Massague J, Brivanlou AH. 2006. Unique players in the BMP pathway: Small C-terminal domain phosphatases dephosphorylate Smad1 to attenuate BMP signaling. Proc Natl Acad Sci USA 103:11940–11945.

Kodaira K, Imada M, Goto M, Tomoyasu A, Fukuda T, Kamijo R, Suda T, Higashio K, Katagiri T. 2006. Purification and identification of a BMP-like factor from bovine serum. Biochem Biophys Res Commun 345:1224–1231.

Kokabu S, Ohte S, Sasanuma H, Shin M, Yoneyama K, Murata E, Kanomata K, Nojima J, Ono Y, Yoda T, Fukuda T, Katagiri T. 2011. Suppression of BMP-Smad signaling axis-induced osteoblastic differentiation by small C-terminal domain phosphatase 1, a Smad phosphatase. Mol Endocrinol 25:474–481.

Kurisaki K, Kurisaki A, Valcourt U, Terentiev AA, Pardali K, Ten Dijke P, Heldin CH, Ericsson J, Moustakas A. 2003. Nuclear factor YY1 inhibits transforming growth factor beta- and bone morphogenetic protein-induced cell differentiation. Mol Cell Biol 23:4494–4510.

Komatsu M, Chiba T, Tatsumi K, Iemura S, Tanida I, Okazaki N, Ueno T, Kominami E, Natsume T, Tanaka K. 2004. A novel protein-conjugating system for Ufm1, a ubiquitin-fold modifier. EMBO J 23:1977–1986.

Lin X, Duan X, Liang YY, Su Y, Wrighton KH, Long J, Hu M, Davis CM, Wang J, Brunicardi FC, Shi Y, Chen YG, Meng A, Feng XH. 2006. PPM1A functions as a Smad phosphatase to terminate TGFbeta signaling. Cell 125:915–928.

Loughlin FE, Mansfield RE, Vaz PM, McGrath AP, Setiyaputra S, Gamsjaeger R, Chen ES, Morris BJ, Guss JM, Mackay JP. 2009. The zinc fingers of the SR-like protein ZRANB2 are single-stranded RNA-binding domains that recognize 5' splice site-like sequences. Proc Natl Acad Sci USA 106:5581–5586.

Mangs AH, Morris BJ. 2008. ZRANB2: Structural and functional insights into a novel splicing protein. Int J Biochem Cell Biol 40:2353–2357.

Miyazono K, Maeda S, Imamura T. 2005. BMP receptor signaling: Transcriptional targets, regulation of signals, and signaling cross-talk. Cytokine Growth Factor Rev 16:251–263.

Miyazono K, Maeda S, Imamura T. 2006. Smad Transcriptional Co-activators and Co-repressors. In: Ten Dijke P, Heldin CH, editors Smad signal transduction. Dordrecht Netherlands: Springer. pp 277–293.

Nakamura Y, Weidinger G, Liang JO, Aquilina-Beck A, Tamai K, Moon RT, Warman ML. 2007. The CCN family member Wisp3, mutant in progressive pseudorheumatoid dysplasia, modulates BMP and Wnt signaling. J Clin Invest 117:3075–3086.

Natsume T, Yamauchi Y, Nakayama H, Shinkawa T, Yanagida M, Takahashi N, Isobe T. 2002. A direct nanoflow liquid chromatography-tandem mass spectrometry system for interaction proteomics. Anal Chem 74:4725–4733.

Nojima J, Kanomata K, Takada Y, Fukuda T, Kokabu S, Ohte S, Takada T, Tsukui T, Yamamoto TS, Sasanuma H, Yoneyama K, Ueno N, Okazaki Y, Kamijo R, Yoda T, Katagiri T. 2010. Dual roles of smad proteins in the conversion from myoblasts to osteoblastic cells by bone morphogenetic proteins. J Biol Chem 285:15577–15586.

Ohte S, Shin M, Sasanuma H, Yoneyama K, Akita M, Ikebuchi K, Jimi E, Maruki Y, Matsuoka M, Namba A, Tomoda H, Okazaki Y, Ohtake A, Oda H, Owan I, Yoda T, Furuya H, Kamizono J, Kitoh H, Nakashima Y, Susami T, Haga N, Komori T, Katagiri T. 2011. A novel mutation of ALK2, L196P, found in the most benign case of fibrodysplasia ossificans progressiva activates BMP-specific intracellular signaling equivalent to a typical mutation, R206H. Biochem Biophys Res Commun 407:213–218.

Shen H, Green MR. 2006. RS domains contact splicing signals and promote splicing by a common mechanism in yeast through humans. Genes Dev 20:1755–1765.

Suzuki A, Thies RS, Yamaji N, Song JJ, Wozney JM, Murakami K, Ueno N. 1994. A truncated bone morphogenetic protein receptor affects dorsal-ventral patterning in the early Xenopus embryo. Proc Natl Acad Sci USA 91:10255–10259.

Suzuki T, Fujisawa JI, Toita M, Yoshida M. 1993. The trans-activator tax of human T-cell leukemia virus type 1 (HTLV-1) interacts with cAMP-responsive element (CRE) binding and CRE modulator proteins that bind to the 21-base-pair enhancer of HTLV-1. Proc Natl Acad Sci USA 90:610–614.

Urist MR. 1965. Bone: Formation by autoinduction. Science 150:893–899.

Wan M, Cao X. 2005. BMP signaling in skeletal development. Biochem Biophys Res Commun 328:651–657.

Wiemann S, Weil B, Wellenreuther R, Gassenhuber J, Glassl S, Ansorge W, Bocher M, Blocker H, Bauersachs S, Blum H, Lauber J, Dusterhoft A, Beyer A, Kohrer K, Strack N, Mewes HW, Ottenwalder B, Obermaier B, Tampe J, Heubner D, Wambutt R, Korn B, Klein M, Poustka A. 2001. Toward a catalog of human genes and proteins: Sequencing and analysis of 500 novel complete protein coding human cDNAs. Genome Res 11:422–435.

Wu JW, Krawitz AR, Chai J, Li W, Zhang F, Luo K, Shi Y. 2002. Structural mechanism of Smad4 recognition by the nuclear oncoprotein Ski: Insights on Ski-mediated repression of TGF-beta signaling. Cell 111:357–367.

Yu PB, Deng DY, Lai CS, Hong CC, Cuny GD, Bouxsein ML, Hong DW, McManus PM, Katagiri T, Sachidanandan C, Kamiya N, Fukuda T, Mishina Y, Peterson RT, Bloch KD. 2008a. BMP type I receptor inhibition reduces heterotopic ossification. Nat Med 14:1363–1369.

Yu PB, Hong CC, Sachidanandan C, Babitt JL, Deng DY, Hoyng SA, Lin HY, Bloch KD, Peterson RT. 2008b. Dorsomorphin inhibits BMP signals required for embryogenesis and iron metabolism. Nat Chem Biol 4:33–41.

Zhu H, Kavsak P, Abdollah S, Wrana JL, Thomsen GH. 1999. A SMAD ubiquitin ligase targets the BMP pathway and affects embryonic pattern formation. Nature 400:687–693.

Microbiology and Immunology

Microbiol Immunol 2012; **56**: 99–106
doi:10.1111/j.1348-0421.2012.00412.x

ORIGINAL ARTICLE

Reactivity of human convalescent sera with influenza virus hemagglutinin protein mutants at antigenic site A

Eri Nobusawa, Katsumi Omagari, Setsuko Nakajima and Katsuhisa Nakajima

Department of Virology, Nagoya City University Graduate School of Medical Science, Nagoya City, Aichi, Japan

ABSTRACT

How the antibodies of individual convalescent human sera bind to each amino acid residue at the antigenic sites of hemagglutinin (HA) of influenza viruses, and how the antigenic drift strains of influenza viruses are selected by human sera, is not well understood. In our previous study, it was found by a binding assay with a chimeric HA between A/Kamata/14/91 (Ka/91) and A/Aichi/2/68 that convalescent human sera, following Ka/91 like (H3N2) virus infection, bind to antigenic site A of Ka/91 HA. Here using chimeric HAs possessing single amino acid substitutions at site A, it was determined how those human sera recognize each amino acid residue at antigenic site A. It was found that the capacity of human sera to recognize amino acid substitutions at site A differs from one person to another and that some amino acid substitutions result in all convalescent human sera losing their binding capacity. Among these amino acid substitutions, certain ones might be selected by chance, thus creating successive antigenic drift. Phylogenetic analysis of the drift strains of Ka/91 showed amino acid substitutions at positions 133, 135 and 145 were on the main stream of the phylogenetic tree. Indeed, all of the investigated convalescent sera failed to recognize one of them.

Key words antigenic drift, hemagglutinin, human sera.

Influenza is an acute infectious respiratory disease caused by influenza viruses. To date, vaccines have failed to control influenza and epidemics occur every winter season. Influenza virus has a remarkable ability to escape host defense mechanisms by altering the antigenic character of its HA and NA proteins, especially through changes in amino acid residues on the HA molecule. In order to find ways to control influenza epidemics, it is important to elucidate the molecular mechanisms by which viruses alter their antigenic character and thus escape from human anti-sera. Analyses of natural and laboratory-selected antigenic variants have resulted in identification of four to five antigenic sites on the HA protein of influenza A (H3N2) viruses (1–3).

Longstanding observations have demonstrated the role of serum antibodies to HA protein in protecting against infection (4–6). Serum antibodies are also important in recovery from influenza virus infection (7–9). The specificity with which human serum antibodies bind to antigenic sites on the HA protein varies considerably from person to person (10, 11), suggesting that antigenic variants may arise in individuals who are only partially immunized (i.e. who have not developed antibodies to all antigenic sites) and are susceptible to mutants in which only one or two antigenic sites have been changed (12). The question is how, under immune pressure, are the amino acid substitutions that distinguish drift strains from the original strain selected.

Correspondence
Eri Nobusawa, Influenza Virus Research Center, National Institute of Infectious Diseases, 4–7–1, Gakuen, Musashi Murayama-shi, Tokyo, 208–0011, Japan.
Tel: +81 42 848 7168; fax: +81 42 561 6124; email: nobusawa@nih.go.jp

Received 3 August 2011; revised 5 December 2011; accepted 8 December 2011.

List of Abbreviations: Ai, Aichi; HA, hemagglutinin; HI, hemagglutination inhibition; Ka, Kamata; mAb, monoclonal antibody; MEM, minimal essential medium; NA, neuraminidase; NI, neutralization inhibition; S1, acute phase; S2, convalescent phase.

Researchers have reported that distinct mAbs with different amino acid sequences can recognize the same epitopes on an antigen molecule (6, 13). In their study of anti-HA antibodies, Fleury *et al.* (13) showed that binding of HC45 Fab and BH151 Fab has very similar orientations and positions with regard to the molecule of A/Aichi/2/68 (Ai/68) and displays a similar affinity, but that HC45 interacts with many more amino acid residues on the HA molecule. In experiments with anti-NA antibodies, Malby *et al.* (14) showed that NC10 and NC41 make contact with the NA molecule through a common set of residues but most of the interactions with these residues differ sterically and chemically between the two complexes.

Even when they are raised against a similar antigen and recognize the same antigenic site, the amino acid sequences of the antigen binding-region on neutralizing antibodies may differ from person to person. Therefore, at the antigenic sites of HA, amino acid residues that interact with individual neutralizing antibodies may also vary from person to person. If individual antibodies recognize the corresponding antigenic sites differently, how are particular amino acid substitutions selected under immune pressures, causing antigenic drift?

We previously reported that a chimeric HA protein method can be used to determine the capacity of human sera to bind to each antigenic site (11) and also showed that semi-quantitative binding of human sera to H3HA correlates with HI activity (16). In that study, we examined the ability of paired sera obtained from eight patients aged 3 to 14 years, who were infected with influenza A (H3N2) virus during 1990–1991, to bind to chimeric HA proteins expressed on COS cells by an expression vector. Individual convalescent sera bound to different antigenic regions of A/Kamata/14/91 (H3N2)(Ka/91) HA: site C/E, site A, site A/B1, site B2 and site C, depending on the patient's age. Recently we analyzed escape mutants selected with mAb203 raised against Ka/91, and found that the amino acid residues at nine positions of antigenic site A of mutants differed from those found in Ka/91 HA (17). To understand how the character of the amino acid residues constituting the epitope affects binding to mAb203, we introduced one-point amino acid substitutions into those nine positions of Ka/91 HA and analyzed their binding to mAb203. We showed that the ability of mAb203 to bind to mutant HA molecules depends on the positions and species of substituted amino acid residues. To extend our knowledge of antigenic drift, in the present study we attempted to discern amino acid substitutions in HA related to antigenic drift of Ka/91. All the convalescent sera used in our previous study showed decreased HI reactivity with drift strains of Ka/91 and five of the convalescent sera bound to site A of Ka/91 HA (11). In regard to the effect of the mutations at site A on the mAb203 binding, we analyzed the binding capacity of those convalescent sera to mutant HAs with one-point mutations at site A similar to those found in the previous study.

MATERIALS AND METHODS

Human sera

Paired sera from four patients aged 12 to 14 years who were infected with influenza A (H3N2) viruses during January to February in 1991 were used (11). The sera of the acute and convalescent phase were collected two to three days and two to three months after the onset of the fever, respectively. The convalescent sera bound only to the chimeric HA Ka91/Ai68, which includes the HA1 region of Ka/91 and the HA2 region of Ai/68, but not to the chimeric HA, Ai68/Ka91, which includes the HA1 region of Ai/68 and the HA2 region of Ka/91(11).

Mouse monoclonal antibodies

Mouse mAbs 203 and 35 directed against the HA protein of Ka/91 were obtained as described previously (11).

Chimeric hemagglutinin cDNAs

cDNA of chimeric HA, #2HA, in which amino acid residues between positions 96 and 150 of Ai/68 HA had been replaced with those of Ka/91 HA (Fig. 1), was cloned into an expression vector pME18s (pME18s-#2HA) as described previously (11).

Site-directed mutagenesis

Site-directed mutations were introduced between amino acid residues at positions 96 to 150 of #2HA using the Mutan-Super Express Km kit (Takara Bio, Shiga, Japan) as follows. Briefly, the PCR product of pME18s-#2HA DNA amplified with primers pME (−) (18) and KO2 (19) was digested with EcoRI and PstI. The EcoRI/PstI fragment was inserted into pKF18k (pKF18k-#2HA) and the desired clones were obtained in JM103 in the presence of kanamycin (0.17 μg/mL). The PCR product of pKf18k-#2HA DNA (8 p mol) amplified with a selection primer (Takara Bio) and a mutant primer was precipitated with NH4-acetate and ethanol, and then dissolved in water. The PCR products were then cloned in MV1184 in the presence of kanamycin (1 μg/mL). Selected mutant cDNAs were digested with EcoRI and NdeI. These fragments were then replaced with the counterpart of #2HA cDNA.

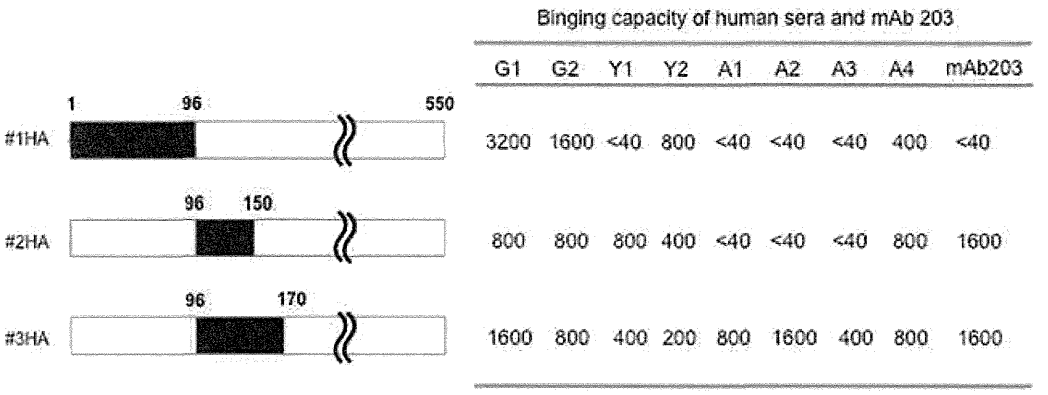

Fig. 1. Binding capacity of each patient's convalescent serum and mAb203 to chimeric HA proteins, #1HA to #3HA. Chimeric HAs expressed on Cos cells were stained with diluted sera and FITC-labeled anti-human goat serum. The binding capacity of the convalescent sera of each patient, G1, G2, Y1, Y2, A1, A2, A3, and A4, was expressed as the highest dilution point at which the expressed HAs were detected by the diluted sera. This figure is prepared partially based on data from a previous study (11).

Immunofluorescent staining of the hemagglutinin protein expressed in COS cells

Transfection was performed as described previously (19, 15). Briefly, each cDNA (200 ng) in MEM was incubated with lipofectamine for 15 min at room temperature. COS cells (0.5×10^5 cells/18 mm coverglass) prepared 18 hr before use were washed with MEM. The DNA and lipofectamine mixture was added to the cells, which were then incubated for 6 hr at 37°C. The medium was changed to MEM containing 10% FCS and the cells were further incubated for 42 hr at 37°C. The cells were then fixed with ethanol–acetone (1:1) at 4 C for 15 min. Indirect immunofluorescent staining was performed with human sera, mouse mAb203 or 35 and FITC-labeled anti-human or anti-mouse goat anti-sera. mAb35, which recognize both the Ka/91and Ai/68 HA proteins, was used to confirm expression of #2HA and mutant HA in the COS cells. For the quantitative FITC assay using diluted human sera, two separate experiments were carried out. The difference in values was not more than twofold and the smaller of the two values was used as described previously (11, 16).

Three-dimensional modeling

To construct a model of the HA protein of Ka/91, the structure of Ai/68 (1HGF.pdb, Protein Data Bank) was modified. Amino acids of Ai/68 were replaced one by one according to the evolution of H3HA until they were the same as those of Ka/91 and the model constructed using CAChe version 6.1 software (Fujitsu, Japan) with the MM2 calculation program. Optimization continued until the energy change became less than 0.001 kcal/mol as described previously (17). The model structure of chimerical #2HA was also constructed using the method described above.

RESULTS

Characteristics of convalescent human sera and mAb203 raised against Ka/91

In our previous study, we investigated the binding properties to Ka/91-HA of eight paired sera collected during S1 and S2 from patients infected with Ka/91-like viruses during influenza season 1991/1992 (11). In brief, we created chimeric HAs by connecting Ka/91(black) and Ai/68 (white) HA at the indicated positions of the amino acid sequence numbers (Fig. 1). #1HA includes parts of antigenic site C and E of Ka/91HA. #2HA and #3HA include antigenic site A, and antigenic sites A and B1 of Ka/91HA, respectively. We stained each chimeric HA expressed on COS cells with serially diluted patient sera and FITC-labeled anti-human goat serum; the binding capacity of antibodies in the sera to the other antigenic sites of KA/91-HA could be disregarded. We found the convalescent sera of four patients (G1, G2 Y2, and A4), five patients (G1, G2, Y1, Y2 and A4), and all patients bound to the antigenic site(s) C/E, A, and A/B1, respectively (Fig. 1).

In this study, we used G1, G2, Y1 and Y2 sera to investigate the influence of amino acid substitutions at site A of Ka/91-HA on the binding capacity of human sera. We introduced the following one-point amino acid substitutions into the antigenic site A of the chimeric #2HA: A131D, A131T, G142E, G142R, G142V, G142S, S143P, V144I and S146N.

Amino acid substitutions in the HA1 region of Ka/91 occur at 14% of the HA1 positions in Ai/68. Therefore,

the fine structures of these two HAs might be different. We used molecular mechanics calculations to model the structure of Ka/91 and chimeric #2HA based on the Ai/68-HA structure (Fig. 2). The modeled structures of their antigenic site A were not so different from that of Ai/68-HA. Amino acid residues from Ka/91 (yellow), including site A (green) and mutated positions (red and purple) are indicated on the structure of chimeric #2HA.

Differences in the binding properties of mAb203 to chimeric #2HA mutants carrying one-point amino acid substitutions at site A depend on the character of the substituted amino acid residues. There are negative mutations, A131D, A131T, G142E, G142R, G142V, G142S, and S143P, and positive mutations, V144I and S146N. The former were not recognized. However, the latter were recognized by mAb203, which is the same result as that of our previous study using full Ka/91-HA (17).

The binding properties of human convalescent sera to amino acid residues at site A on the H3HA protein

We confirmed the extent of expression of mutant HA on COS cells by indirect immunofluorescent staining using mAb35, which recognizes both Ka/91 and Ai/68 HA. We stained all mutant HAs by mAb35 diluted 3200- to 6400-fold. We performed semi-quantitative analysis of the binding capacity by determining the limiting dilution for each human convalescent serum by indirect immunofluorescent staining. All human sera bound to chimeric #2HA equally with a binding capacity up to 1:800. However, their binding capacity to each mutant HA differed from person to person according to the character and positions of the substituted amino acid residues (Table 1), that is, G1, G2, and Y1 exhibited a binding capacity to A131D up to a dilution of 1:400 to 1:800, but Y2 and mAb203 did not. As for amino acid substitutions at position 142, the binding capacity of G1 to the mutant HAs depended on the substituted amino acid residues, but that of Y1 and Y2 to mutant HAs decreased regardless of the substituted amino acids. Similar to the reactivity of mAb203, all sera lost or decreased their binding capacity to mutant HAs with A131T and G142E (Table 1). This observation suggests that amino acid substitutions to which most sera lose their binding ability might be selected among field strains.

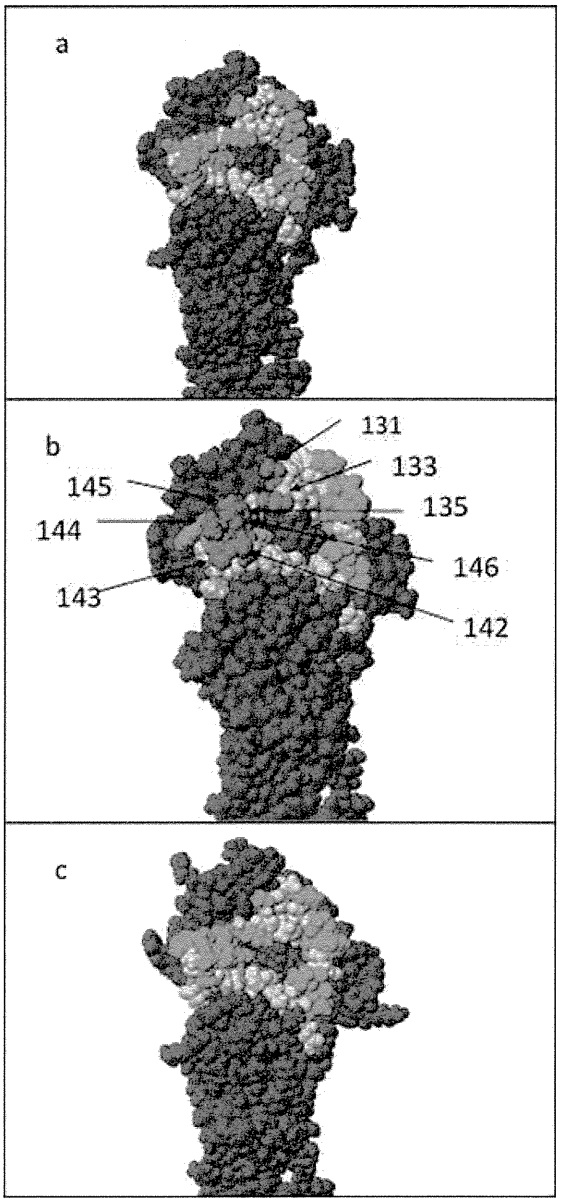

Fig. 2. Three-dimensional structure of HA models, (a) Ai/68 HA, (b) chimeric #2HA, and (c) Ka/91 HA. Three-dimensional HA models of Ka/91 and #2HA were constructed using a molecular mechanics calculation method as described in Materials and Methods. The chimeric structure was constructed by replacement of residues 96–150 (yellow) including site A (green) of Ai68 with those of Ka91 using CAChe software (version 6.1) with the MM2 calculation program. The positions of the one-point mutations are shown in red and purple.

Hemagglutination inhibition reactivity of human sera and mAb203 to field strains

A summary of results of assessing the reactivity of human sera to field strains by the HI test is shown in Table 2. Only the convalescent sera reacted with Ka/91, A/Chiba/54/92, and A/Aichi/12/92 viruses but they did not react with the drift strains of Ka/91, A/Aichi/4/93, A/Aichi/48/93 and A/Aichi/2/94 viruses. As shown in Table 2, mAb203 also had reduced reactivity to these drift strains. Since these human sera and mAb203 bind to site A, the amino acid changes at site A on HA of the drift strains are responsible for the reduced reactivity.

Table 1. Comparison of the binding capacity of each human convalescent serum and monoclonal antibodies to mutant HA

Mutant HAs† with amino acid changes	Human convalescent sera				Monoclonal antibodies	
	G1	G2	Y1	Y2	203	35
#2HA‡	800	800	800	800	3200	6400
A131D	800	800	400	100	<100	3200
A131T	<50	<50	<50	100	<100	1600
G142E	100	<50	<50	<50	<100	1600
G142R	800	800	<100	<100	<100	3200
G142V	200	200	100	<100	<100	6400
G142S	1600	200	200	200	<100	6400
S143P	800	<100	<100	<100	100	6400
V144I	1600	<100	800	200	1600	6400
S146N	800	<100	400	<100	400	6400
S133D§	800	400	800	<100	1600	6400
D135G§	800	400	400	400	1600	3200
K145N§	100	<100	200	<100	100	3200

†, chimeric #2 HA with one-point amino acid changes that were found in drift strains or escape mutants from mAb203; ‡, chimeric #2HA without mutations; §, the same mutation was found in the drift strains of Ka/91 virus.

Table 2. HI titers of patient sera and monoclonal antibody 203 (mAb203) against natural isolates (H3N2) between 1990 and 1994

Sera†	Age (years)	Natural isolates					
		Kamata/14/91	Aichi/12/92	Chiba/54/92	Aichi/4/93	Aichi/48/93	Aichi/2/94
G1-S1	14	20	20	20	20	20	20
G1-S2		320	320	320	40	40	40
G2-S1	12	20	20	20	20	20	20
G2-S2		320	320	320	80	80	80
Y1-S1	12	20	20	20	20	20	20
Y1-S2		160	160	160	20	20	20
Y2-S1	12	20	20	20	20	20	20
Y2-S2		160	160	160	40	40	40
mAb203		6400	NT	6400	<100	<100	<100

†, human sera of S1 and S2 after A/Kamata/14/91 infection. None of these patients had a history of vaccination. NT = Not tested.

Comparison of the amino acid sequences of field isolates collected during 1991 to 1994 seasons

In order to identify the amino acid substitutions responsible for the reduction of HI ability of human sera to the HA of A/Aichi/4/93, A/Aichi/48/93 and A/Aichi/2/94 viruses, we compared the amino acid sequences of the site A region between these three viruses' HAs and Ka/91 HA. Amino acid differences were found at positions 133, 135 and 145 (Fig. 3). To investigate the role of these amino acid changes in the antigenic drift of Ka/91 virus, we examined the phylogenetic relationships among the HAs of 36 natural isolates collected between 1991 and 1994 (sequences of the HA proteins were randomly selected from an influenza sequence data bank) by comparing the amino acid sequences of site A. The viruses were divided into two distinct groups, I and II (Fig. 4), which are distinguished from each other by their respective amino acid substitutions at positions 133(S to D)(S133D), 135(D/E to G/K), and 145(K to N)(K145N) of site A. The antigenic difference at site A on HA between group I and group II viruses may depend on the amino acid changes at these positions.

The amino acid changes responsible for antigenic drift of Ka/91 virus

To study the relationship between amino acid changes found in drift strains and the reduced HI reactivity of human sera and mAb203 with these strains, we further investigated the binding capacity of human convalescent sera to #2HA mutants with one-point amino acid substitutions S133D, D135G or K145N (Table 1). All sera but

```
          96                                                          150
Kamata14  NCYPYDVPDYASLRSLVASSGTLEFINEDFNWTGVAQSGDSYACKRGSVKSFFSR
Chiba54   ..........................T.............E..............
Aichi12   ..........................T.............E..............
Aichi4    ....................................D.G.........N.....
Aichi48   ....................................D.K.........N.....
Aichi2    ....................................D.K....R....N.....
          ************************.*********** * ****.**** *****
```

Fig. 3. Comparison of amino acid sequences between positions 96 and 150 of HA among field isolates. Amino acid sequences of Ka91-like viruses and its drift strains are aligned as follows: Ka91 (Kamata14), A/Chiba/54/92 (Chiba54), A/Aichi/12/92 (Aichi12), A/Aichi/4/93 (Aichi4), A/Aichi/48/93 (Aichi48), and A/Aichi/12/92 (Aichi12) viruses.

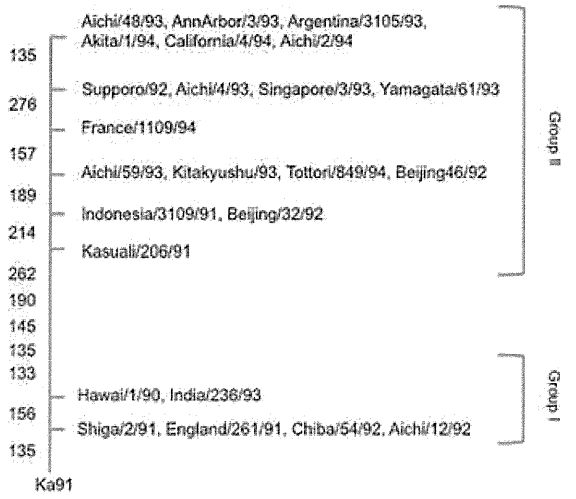

Fig. 4. Phylogenetic relationships among human H3N2 influenza viruses isolated from 1991 through 1994. The numbers on the mainstream designate the positions where we observed amino acid differences compared to Ka91. We divided the viruses into two distinct groups, group I and group II, according to their amino acid sequences.

Y2 bound to the mutant HAs with S133D and D135G. On the other hand, all sera showed lost/decreased binding to mutant HA with K145N (Table 1). mAb203 bound to the mutant HAs with S133D and D135G, but not to mutant HA with K145N.

DISCUSSION

Human serum is polyclonal, containing a mixture of antibodies that recognize different antigenic sites. The binding abilities of human sera used in the current experiments have already been reported in terms of their binding to sites C/E, A and B1 (G1, G2, and Y2), and sites A and B1 (Y1) (11). In addition, the present study showed that these anti-HA sera had different binding capacities to each mutant HA possessing an amino acid substitution at site A of Ka/91 HA. However, it is difficult to say whether the sera used in the present experiments consisted of mixed antibodies or of one main antibody reacting with site A. In any case, anti-HA antibodies induced in human sera by infection with Ka/91-like virus had different binding capacities to Ka/91 HA with substituted amino acid residues at site A.

In these experiments, because escape mutants from mAb203 contain amino acid substitutions only in the A2 and A3 subsites, and because amino acid differences at site A on the HA proteins of group I and II viruses have been observed only in A2 and A3, we introduced amino acid substitutions into the A2 (at positions 133–137) and A3 (at positions 142–147) subsites, but not into the A1 (at positions 121–126) subsite. As shown in Table 1, each human serum had a different binding capacity against each mutant HA with a substituted amino acid at site A on Ka/91 HA.

The different responses of each of the human antibodies to each amino acid substitution may depend on the particular characteristics of the antibody in regard to recognizing its own epitope. The antigenic change found at site A of group II viruses depends mainly on the amino acid substitution K145N. Additional changes at 133 and 135 may strengthen the likelihood of escape. Several authors have shown that, in antigenic drift, amino acid changes at more than two residues on the same antigenic site are common (20, 12). Referring to another antigenic site, in our previous study we happened to find that the amino acid change E156K at site B1 of chimeric #3HA reduced the binding ability of three patient sera to mutant HA. We found this amino acid change in several drift strains of Ka/91. Therefore, another amino acid change, E156K might also relate to antigenic drift of Ka/91. Clarification of the mechanism of antigenic drift by studying these chimeric HA with amino acid mutations and comprehensively analyzing many human convalescent sera for their

reactivities with all antigenic sites or mutant HA, and the breadth of responses to these, is yet to be undertaken.

Can the reason for selection of K145N among various natural isolates be determined? Amino acid substitutions A131T and G142E reduce the binding capacity of each human serum to a similar or greater extent than K145N. K145N occurred due to a transversional change in the genetic code from aaa to aac while A131T is due to a transitional change from gct to act. Arnold and Cameron have reported that RNA polymerase does not have a proofreading mechanism and has different frequencies of transition and transversion (21). *In vitro*, among the escape mutants from monoclonal antibodies against Ka/91 the number of transitional substitutions is reportedly double that of transversional ones (17). Regarding K145N, we expected amino acid substitutions to be selected by chance from the several restricted amino acid substitutions, regardless of the base substitutions in the corresponding codons.

In considering the escape of antigenic variants from human sera, we should take into account the neutralizing activity of each human serum. The different binding activities of each serum may correlate with differences in their HI reactivity because: (i) the sera used showed HI reactivity with Ka/91 virus (11); and (ii) semi-quantitative values of human sera in regard to binding to the HA1 region do correlate with HI titers (16).

Group I viruses may have played a major role in 1991 epidemics but they gradually decreased in importance in the 1992 and 1993 influenza seasons, group II viruses becoming the major strains at that time. Pressure from antisera may explain these phenomena. Human sera from group I virus-infected individuals barely neutralized group II viruses (Table 2); therefore, the latter strains may have been selected by antisera against group I viruses. In this report, we suggest that anti-HA antibodies differ from person to person and the response of an antibody to an amino acid substitution at antigenic sites also varies among individuals. Some amino acid substitutions caused all convalescent human sera to lose their binding capacity. We suspect that amino acid substitutions for successive antigenic drift were selected by chance from these several restricted amino acid substitutions.

ACKNOWLEDGMENTS

We are greatly indebted to J. Mosher for critical editing of the manuscript. We thank K. Maruyama for generously providing the pME18S expression vector. Finally, we are grateful to H. Kojima for her excellent technical assistance. This work was partially supported by a Health and Labor Sciences Research Grants from the Ministry of Health, Labor and Welfare of Japan.

DISCLOSURE

No authors have any conflicts of interest to disclose.

REFERENCES

1. Webster R.G., Laver W.G. (1980) Determination of the number of nonoverlapping antigenic areas on Hong Kong (H3N2) influenza virus hemagglutinin with monoclonal antibodies and the selection of variants with potential epidemiological significance. *Virology* **104**: 139–48.
2. Wiley D.C., Wilson I.A., Skehel J.J. (1981) Structural identification of the antibody-binding sites of Hong Kong influenza haemagglutinin and their involvement in antigenic variation. *Nature* **289**: 373–8.
3. Underwood P.A. (1982) Mapping of antigenic changes in the haemagglutinin of Hong Kong influenza (H3N2) strains using a large panel of monoclonal antibodies. *J Gen Virol* **62**:(Pt 1): 153–69.
4. Couch R.B., Kasel J.A. (1983) Immunity to influenza in man. *Annu Rev Microbiol* **37**: 529–49.
5. Dowdle W.R., Coleman M.T., Mostow S.R., Kaye H.S., Schoenbaum, S.C. (1973) Inactivated influenza vaccines. 2. Laboratory indices of protection. *Postgrad Med J* **49**: 159–63.
6. Hobson D., Curry R.L., Beare A.S., Ward-Gardner A. (1972) The role of serum haemagglutination-inhibiting antibody in protection against challenge infection with influenza A2 and B viruses. *J Hyg (Lond)* **70**: 767–77.
7. Epstein S.L., Misplon J.A., Lawson C.M., Subbarao E.K., Connors M., Murphy B.R. (1993) Beta 2-microglobulin-deficient mice can be protected against influenza A infection by vaccination with vaccinia-influenza recombinants expressing hemagglutinin and neuraminidase. *J Immunol* **150**: 5484–93.
8. Gerhard W., Mozdzanowska K., Furchner M., Washko G., Maiese, K. (1997) Role of the B-cell response in recovery of mice from primary influenza virus infection. *Immunol Rev* **159**: 95–103.
9. Palladino G., Mozdzanowska K., Washko G., Gerhard W. (1995) Virus-neutralizing antibodies of immunoglobulin G (IgG) but not of IgM or IgA isotypes can cure influenza virus pneumonia in SCID mice. *J Virol* **69**: 2075–81.
10. Wang M.L., Skehel J.J., Wiley D.C. (1986) Comparative analyses of the specificities of anti-influenza hemagglutinin antibodies in human sera. *J Virol* **57**: 124–8.
11. Nakajima S., Nobusawa E., Nakajima K. (2000) Variation in response among individuals to antigenic sites on the HA protein of human influenza virus may be responsible for the emergence of drift strains in the human population. *Virology* **274**: 220–31.
12. Wilson I.A., Cox N.J. (1990) Structural basis of immune recognition of influenza virus hemagglutinin. *Annu Rev Immunol* **8**: 737–71.
13. Fleury D., Daniels R.S., Skehel J.J., Knossow M., Bizebard T. (2000) Structural evidence for recognition of a single epitope by two distinct antibodies. *Proteins* **40**: 572–8.
14. Malby R.L., Tulip W.R., Harley V.R., Mckimm-Breschkin J.L., Laver W.G., Webster R.G., Colman P.M. (1994) The structure of a complex between the NC10 antibody and influenza virus neuraminidase and comparison with the overlapping binding site of the NC41 antibody. *Structure* **2**: 733–46.
15. Nobusawa E., Ishihara H., Morishita T., Sato K., Nakajima K. (2000) Change in receptor-binding specificity of recent human influenza A viruses (H3N2): a single amino acid change in hemagglutinin altered its recognition of sialyloligosaccharides. *Virology* **278**: 587–96.
16. Sato K., Morishita T., Nobusawa E., Tonegawa K., Sakae K., Nakajima S., Nakajima K. (2004) Amino-acid change on the

antigenic region B1 of H3 haemagglutinin may be a trigger for the emergence of drift strain of influenza. *A virus J Epidemiol Infect* **132**: 399–406.
17. Nakajima S., Nakajima K., Nobusawa E., Zhao J., Tanaka S., Fukuzawa K. (2007) Comparison of epitope structures of H3HAs through protein modeling of influenza A virus hemagglutinin: mechanism for selection of antigenic variants in the presence of a monoclonal antibody. *Microbiol Immunol* **51**: 1179–87.
18. Nakajima K., Nobusawa E., Tonegawa K., Nakajima S. (2003) Restriction of amino acid change in influenza A virus H3HA: comparison of amino acid changes observed in nature and in vitro. *J Virol* **77**: 10088–98.
19. Nakajima K., Nobusawa E., Nagy A., Nakajima, S. (2005) Accumulation of amino acid substitutions promotes irreversible structural changes in the hemagglutinin of human influenza AH3 virus during evolution. *J Virol* **79**: 6472–7.
20. Plotkin J.B., Dushoff J., Levin S.A. (2002) Hemagglutinin sequence clusters and the antigenic evolution of influenza A virus. *Proc Natl Acad Sci U S A* **99**: 6263–8.
21. Arnold J.J., Cameron C.E. (2004) Poliovirus RNA-dependent RNA polymerase (3Dpol): pre-steady-state kinetic analysis of ribonucleotide incorporation in the presence of Mg2+. *Biochemistry* **43**: 5126–37.

PLOS ONE

Critical Role of an Antiviral Stress Granule Containing RIG-I and PKR in Viral Detection and Innate Immunity

Koji Onomoto[1,2,9¤], Michihiko Jogi[1,3,4], Ji-Seung Yoo[1,3], Ryo Narita[1], Shiho Morimoto[1], Azumi Takemura[1], Suryaprakash Sambhara[5], Atushi Kawaguchi[6,7], Suguru Osari[6], Kyosuke Nagata[6], Tomoh Matsumiya[8], Hideo Namiki[9], Mitsutoshi Yoneyama[4,10]*, Takashi Fujita[1,3]*

1 Laboratory of Molecular Genetics, Institute for Virus Research, Kyoto University, Kyoto, Japan, **2** Research Institute for Science and Engineering, Waseda University, Tokyo, Japan, **3** Laboratory of Molecular Cell Biology, Graduate School of Biostudies, Kyoto University, Kyoto, Japan, **4** Division of Molecular Immunology, Medical Mycology Research Center, Chiba University, Chuo-ku, Chiba, Japan, **5** Influenza Division, Centers for Disease Control and Prevention, Atlanta, Georgia, United States of America, **6** Department of Infection Biology, Faculty of Medicine and Graduate School of Comprehensive Human Sciences, University of Tsukuba, Tsukuba, Japan, **7** Kitasato Institute for Life Sciences, Kitasato University, Tokyo, Japan, **8** Department of Vascular Biology, Institute of Brain Science, Graduate School of Medicine, Hirosaki University, Aomori, Japan, **9** Graduate School of Science and Engineering, Waseda University, Tokyo, Japan, **10** PRESTO, Japan Science and Technology Agency, Honcho Kawaguchi, Saitama, Japan

Abstract

Retinoic acid inducible gene I (RIG-I)-like receptors (RLRs) function as cytoplasmic sensors for viral RNA to initiate antiviral responses including type I interferon (IFN) production. It has been unclear how RIG-I encounters and senses viral RNA. To address this issue, we examined intracellular localization of RIG-I in response to viral infection using newly generated anti-RIG-I antibody. Immunohistochemical analysis revealed that RLRs localized in virus-induced granules containing stress granule (SG) markers together with viral RNA and antiviral proteins. Because of similarity in morphology and components, we termed these aggregates antiviral stress granules (avSGs). Influenza A virus (IAV) deficient in non-structural protein 1 (NS1) efficiently generated avSGs as well as IFN, however IAV encoding NS1 produced little. Inhibition of avSGs formation by removal of either the SG component or double-stranded RNA (dsRNA)-dependent protein kinase (PKR) resulted in diminished IFN production and concomitant enhancement of viral replication. Furthermore, we observed that transfection of dsRNA resulted in IFN production in an avSGs-dependent manner. These results strongly suggest that the avSG is the locus for non-self RNA sensing and the orchestration of multiple proteins is critical in the triggering of antiviral responses.

Citation: Onomoto K, Jogi M, Yoo J-S, Narita R, Morimoto S, et al. (2012) Critical Role of an Antiviral Stress Granule Containing RIG-I and PKR in Viral Detection and Innate Immunity. PLoS ONE 7(8): e43031. doi:10.1371/journal.pone.0043031

Editor: Akio Kanai, Keio University, Japan

Received April 11, 2012; **Accepted** July 16, 2012; **Published** August 13, 2012

Funding: The Ministry of Education, Culture, Sports, Science and Technology in Japan (Innovative Areas "RNA regulation" (No.20112009), Scientific Research "A", and Research Activity Start-up) (http://www.mext.go.jp/english/), the Ministry of Health, Labour and Welfare of Japan (http://www.mhlw.go.jp/english/index.html), the PRESTO Japan Science and Technology Agency (http://www.jst.go.jp/kisoken/presto/index_e.html), the Uehara Memorial Foundation (http://www.ueharazaidan.com/), the Mochida Memorial Foundation for Medical and Pharmaceutical Research (http://www.mochida.co.jp/zaidan/), the Takaeda Science Foundation (http://www.takeda-sci.or.jp/index.html), the Naito Foundation (http://www.naito-f.or.jp/), and Nippon Boehringer Ingelheim (http://www.boehringer-ingelheim.co.jp/com/Home/index.jsp). The funders had no role in study design, data collection and analysis, decision to publish, or preparation of the manuscript.

Competing Interests: The authors have the following competing interests: This study was partly funded by Nippon Boehringer Ingelheim. There are no patents, products in development or marketed products to declare. This does not alter the authors' adherence to all the PLoS ONE policies on sharing data and materials, as detailed online in the guide for authors.

* E-mail: myoneyam@faculty.chiba-u.jp (MY); tfujita@virus.kyoto-u.ac.jp (TF)

¤ Current address: Division of Molecular Immunology, Medical Mycology Research Center, Chiba University, Chuo-ku, Chiba, Japan

Introduction

Type I and III interferons (IFNs) are cytokines with strong antiviral activity [1,2]. Upon the binding of IFNs with their cognate receptor complexes, an intracellular signal is activated resulting in the activation of transcription factors, IFN stimulated gene factor 3, heterotrimer of signal transducer and activator of transcription (STAT)1, STAT2, and IFN regulatory factor (IRF)-9, and STAT1 homodimer. These factors induce the activation of hundreds of interferon stimulated genes (ISGs). Some of the ISG products act as antiviral proteins and participate in the blockade of viral replication. The level of double-stranded (ds) RNA-dependent protein kinase (PKR) is enhanced by IFN treatment, however catalytic activity of PKR requires dsRNA. When IFN-treated cells are infected by virus, dsRNA, produced as a by-product of viral replication, activates PKR, and the activated PKR inactivates eukaryotic translation initiation factor (eIF) 2á by phosphorylation [3]. Another antiviral protein 2′–5′ oligoadenylate synthetase (OAS) is also induced to express by IFN. Catalytic activity of OAS requires dsRNA and virus infection activates OAS to produce 2′–5′ A. 2′–5′ A then activates cellular RNase L, and viral RNA is degraded [1]. Although, the "dsRNA-activated inhibition" model is widely accepted, IFN-treated and virus-infected cells do not necessarily undergo suicide, as conventional IFN bioassays have demonstrated IFN-induced survival of infected cells [4]. To explain these phenomena, it has been hypothesized that viral transcription/translation takes place in a specific subcellular compartment, thus the blocking of translation and the degradation